Electron-photon exchange-correlation approximation for quantum-electrodynamical density-functional theory

I-Te Lu [1,*] Michael Ruggenthaler [1,†] Nicolas Tancogne-Dejean [1] Simone Latini [1,2] Markus Penz [1,3] and Angel Rubio [1,4,‡]

[1]*Max Planck Institute for the Structure and Dynamics of Matter and Center for Free-Electron Laser Science, Luruper Chaussee 149, 22761 Hamburg, Germany*

[2]*Department of Physics, Technical University of Denmark, 2800 Kgs. Lyngby, Denmark*

[3]*Department of Computer Science, Oslo Metropolitan University, 0130 Oslo, Norway*

[4]*Center for Computational Quantum Physics (CCQ), The Flatiron Institute, 162 Fifth Avenue, New York, New York 10010, USA*

(Received 15 February 2024; accepted 30 April 2024; published 23 May 2024)

Quantum-electrodynamical density-functional theory (QEDFT) provides a promising avenue for exploring complex light-matter interactions in optical cavities for real materials. Similar to conventional density-functional theory, the Kohn-Sham formulation of QEDFT needs approximations for the generally unknown exchange-correlation functional. In addition to the usual electron-electron exchange-correlation potential, an approximation for the electron-photon exchange-correlation potential is needed. A recent electron-photon exchange functional [C. Schäfer *et al.*, Proc. Natl. Acad. Sci. USA **118**, e2110464118 (2021)], derived from the equation of motion of the nonrelativistic Pauli-Fierz Hamiltonian, shows robust performance in one-dimensional systems across weak- and strong-coupling regimes. Yet, its performance in reproducing electron densities in higher dimensions remains unexplored. Here we consider this QEDFT functional approximation from one- to three-dimensional finite systems and across weak to strong light-matter couplings. The electron-photon exchange approximation provides excellent results in the ultrastrong-coupling regime. However, to ensure accuracy also in the weak-coupling regime across higher dimensions, we introduce a computationally efficient renormalization factor for the electron-photon exchange functional, which accounts for part of the electron-photon correlation contribution. These findings extend the applicability of photon-exchange-based functionals to realistic cavity-matter systems, fostering the field of cavity QED (quantum-electrodynamics) materials engineering.

DOI: 10.1103/PhysRevA.109.052823

I. INTRODUCTION

Optical cavities can, under specific conditions, enhance light-matter interaction without strong lasers or external pumping [1–5], enabling precise control over materials properties [6–12]. Recent experimental advancements have allowed researchers to explore the strong, ultrastrong, or even deep-strong light-matter coupling regime [13,14]. On the other hand, in the realm of theoretical techniques for light-matter interactions [1,2,15–17], quantum-electrodynamical density-functional theory (QEDFT) stands out as an efficient and accurate approach for realistic materials [1,18]. Exact QEDFT treats electrons and photons equally, addressing complex computational challenges posed by the large degrees of freedom, in contrast to simpler models that focus on a subset of electronic states.

In practice, a primary challenge of QEDFT is determining, in addition to the standard electron-electron (arising from the longitudinal Coulomb interaction), the electron-photon (transverse interaction) exchange-correlation potential for the noninteracting Kohn-Sham (KS) system to reproduce the electron and photon density of the interacting and coupled system [19]. Various perturbative approximations have emerged [20,21] to obtain the electron-photon exchange potential, including an optimized-effective potential (OEP) method [20] and a recently developed density-based method within first-order perturbation theory [21], which are suitable for realistic molecules [22,23]. Yet, these perturbative approaches lose accuracy in strongly and ultrastrongly coupled systems [22]. To overcome these limitations, nonperturbative methods need to be developed. For instance, a recent method based on the photon-random-phase approximation shows promise for strong coupling in the generalized Dicke model, but its suitability for realistic systems awaits further exploration [24].

Another nonperturbative technique [25], based on the local-force equation of the nonrelativistic Pauli-Fierz (PF) Hamiltonian, approximates electron-photon exchange-correlation potentials by expressing quantum-photon fluctuations in the PF Hamiltonian through the paramagnetic

*i-te.lu@mpsd.mpg.de
†michael.ruggenthaler@mpsd.mpg.de
‡angel.rubio@mpsd.mpg.de

current of the matter system, simplifying the intricate photon Fock-space computations. This technique has been studied for a simple one-dimensional system (e.g., one-dimensional hydrogen with a soft-core Coulomb potential) and accurately reproduces the static total energy, dipole moment, and polariton spectrum, covering the whole range from weak to deep-strong light-matter coupling scenarios. In its simplest form, this approximation strategy results in the electron-photon exchange (px) potential and, in the homogeneous limit, gives a local-density version known as the electron-photon-exchange local-density approximation (pxLDA) functional. Thanks to its density-based pxLDA potential and construction in the velocity gauge, this method is adaptable for both large finite and extended systems. However, its effectiveness in replicating electron densities coupled to optical cavities in higher-dimensional systems remains unexplored.

In this work, we demonstrate the efficacy of the px functional, derived from the local-force equation of the PF Hamiltonian within the long-wavelength approximation, in accurately reproducing the electron density of one-, two-, and three-dimensional finite systems in the ultrastrong-coupling regime. However, as we approach the weak-coupling regime, accounting for the electron-photon correlation becomes essential to ensure accurate qualitative and quantitative electron density predictions. To address this, we propose the inclusion of a renormalization factor in the electron-photon functional. We focus on three finite one-electron systems coupled to the photon vacuum of a perfect cavity: a one-dimensional harmonic oscillator (HO), a two-dimensional quantum ring, and a three-dimensional hydrogen atom. All these systems are coupled to a single effective photon mode [26] for simplicity, but it is straightforward to extend the px potential to many photon modes due to the additive nature of the functional approximation. Emphasizing the electron-photon interaction, our findings provide insights into the performance of the proposed px functional and highlight its importance in predicting light-matter interactions across different materials and scenarios. We note that the electron-photon functional is not limited to, but can be beyond, the long-wavelength approximation and that the extension to the time-dependent case for driven cavities will require developing functionals depending on the time-dependent current operator, which we will show in followup work.

II. METHODOLOGY

A. Nonrelativistic Paul-Fierz Hamiltonian in the long-wavelength approximation

We start with the nonrelativistic PF Hamiltonian $\hat{H}_{\rm PF}$ for N_e electrons interacting with M_p *bare* linearly polarized photon modes within the Coulomb gauge and in *long-wavelength* approximation [26], i.e., the vector potential operator is $\hat{\mathbf{A}}(\mathbf{r}) \to \hat{\mathbf{A}}$. In Hartree atomic units, it is given as

$$\hat{H}_{\rm PF}(t) = \frac{1}{2}\sum_{l=1}^{N_e}\left(-i\nabla_l + \frac{1}{c}\hat{\mathbf{A}}\right)^2 + \frac{1}{2}\sum_{l\neq k}^{N_e} w(\mathbf{r}_l,\mathbf{r}_k) + \sum_{l=1}^{N_e} v_{\rm ext}(\mathbf{r}_l,t) + \sum_{\alpha=1}^{M_p}\omega_\alpha\left(\hat{a}_\alpha^\dagger\hat{a}_\alpha + \frac{1}{2}\right). \quad (1)$$

Here l (α) is the index for electrons (photon modes), $w(\mathbf{r}_l,\mathbf{r}_k)$ the longitudinal Coulomb interaction among electrons, $v_{\rm ext}(\mathbf{r}_l,t)$ an external (potentially time-dependent) scalar external potential due to, e.g., the nuclei, and ω_α and $\hat{a}_\alpha$ ($\hat{a}_\alpha^\dagger$) the bare photon frequency and annihilation (creation) operator for the αth photon mode, respectively. The vector potential operator is

$$\hat{\mathbf{A}} = \sum_{\alpha=1}^{M_p}\hat{A}_\alpha\boldsymbol{\varepsilon}_\alpha = c\sum_{\alpha=1}^{M_p}\lambda_\alpha\boldsymbol{\varepsilon}_\alpha\frac{1}{\sqrt{2\omega_\alpha}}(\hat{a}_\alpha^\dagger + \hat{a}_\alpha),$$

where $\hat{A}_\alpha = (c\lambda_\alpha/\sqrt{2\omega_\alpha})(\hat{a}_\alpha^\dagger + \hat{a}_\alpha)$, and c is the speed of light and $\boldsymbol{\varepsilon}_\alpha$ the polarization of the αth bare linearly polarized photon mode with the light-matter coupling parameter (or mode strength) λ_α, which is proportional to the mode volume V_α via $\sqrt{1/V_\alpha}$.[1] Note that to establish the full mapping underlying QEDFT in the long-wavelength approximation [26], one also adds a mode-resolved external current as a control field for the photonic subsystem [1,18,27,28]. It is straightforward to include the corresponding external and KS currents. Yet, since their effects are mostly important in the time-dependent case we disregard these contributions in the following.

After the expansion of the kinetic term in Eq. (1), the diamagnetic term $\hat{\mathbf{A}}^2$ can be absorbed by redefining the bare photon modes, which become the so-called *dressed* photon modes. The relationship between the bare and dressed photon modes can be found in Appendix A. The PF Hamiltonian in terms of the dressed photon modes becomes

$$\hat{\tilde{H}}_{\rm PF}(t) = -\frac{1}{2}\sum_{l=1}^{N_e}\nabla_l^2 + \frac{1}{2}\sum_{l\neq k}^{N_e} w(\mathbf{r}_l,\mathbf{r}_k) + \sum_{l=1}^{N_e} v_{\rm ext}(\mathbf{r}_l,t) + \frac{1}{c}\hat{\tilde{\mathbf{A}}}\cdot\hat{\mathbf{J}}_p + \sum_{\alpha=1}^{M_p}\tilde{\omega}_\alpha\left(\hat{\tilde{a}}_\alpha^\dagger\hat{\tilde{a}}_\alpha + \frac{1}{2}\right), \quad (2)$$

where $\hat{\tilde{a}}^\dagger$ ($\hat{\tilde{a}}$) is the creation (annihilation) operator, $\tilde{\omega}_\alpha$ photon frequency, $\tilde{\boldsymbol{\varepsilon}}_\alpha$ polarization, and $\tilde{\lambda}_\alpha$ light-matter coupling for the dressed photon modes. The vector potential operator in terms of the dressed photon modes is

$$\hat{\tilde{\mathbf{A}}} = \sum_{\alpha=1}^{M_p}\hat{\tilde{A}}_\alpha\tilde{\boldsymbol{\varepsilon}}_\alpha = c\sum_{\alpha=1}^{M_p}\tilde{\lambda}_\alpha\tilde{\boldsymbol{\varepsilon}}_\alpha\frac{1}{\sqrt{2\tilde{\omega}_\alpha}}(\hat{\tilde{a}}_\alpha^\dagger + \hat{\tilde{a}}_\alpha).$$

Here $\hat{\tilde{A}}_\alpha = (c\tilde{\lambda}_\alpha/\sqrt{2\tilde{\omega}_\alpha})(\hat{\tilde{a}}_\alpha^\dagger + \hat{\tilde{a}}_\alpha)$, and $\hat{\mathbf{J}}_{\rm p} = \sum_{l=1}^{N_e}(-i\nabla_l)$ is the paramagnetic current operator. The light-matter coupling, denoted by λ_α, encodes information about the electromagnetic environment, such as the photon mode volume, and is treated as a free parameter here. To determine whether a system exhibits weak or strong coupling depends on considering both the electronic system and the electromagnetic environment [14,29,30]. Here, we call a system weakly coupled if $\lambda_\alpha/\omega_\alpha \ll 1.0$ and strongly coupled if $\lambda_\alpha/\omega_\alpha \sim 1.0$.

[1] In SI units, λ_α is proportional to $\sqrt{\hbar/V_\alpha\epsilon_0}$ where $\hbar$ and ϵ_0 are the reduced Planck constant and the vacuum permittivity, respectively.

B. Construction of the Kohn-Sham system in the long-wavelength approximation

The many-body PF Hamiltonian with the dressed photon modes [Eq. (2)] in the long-wavelength (dipole) approximation is our starting point for constructing an auxiliary noninteracting KS system within the QEDFT framework [1,18,31], which aims to reproduce the electron density (or current density if we go beyond the long-wavelength approximation and consider full minimal coupling between light and matter) of the original interacting physical system. The auxiliary Hamiltonian we start with is

$$\hat{H}_{\rm s}(t) = \frac{1}{2}\sum_{l=1}^{N_e}\left(-i\nabla_l + \frac{1}{c}\tilde{\mathbf{A}}_{\rm s}(t)\right)^2 + \sum_{l=1}^{N_e} v_{\rm s}(\mathbf{r}_l, t), \quad (3)$$

where $v_{\rm s}(\mathbf{r}, t)$ is an auxiliary potential and $\tilde{\mathbf{A}}_{\rm s}(t) = \sum_{\alpha=1}^{M_p} \tilde{A}_{{\rm s},\alpha}(t)\tilde{\boldsymbol{\varepsilon}}_\alpha$ is an auxiliary classical vector potential (not an operator), constant over space, with [25]

$$\tilde{A}_{{\rm s},\alpha}(t) = -c\int_{-\infty}^{t} \frac{\tilde{\lambda}_\alpha^2}{\tilde{\omega}_\alpha} \sin[\tilde{\omega}_\alpha(t-t')]\tilde{\boldsymbol{\varepsilon}}_\alpha \cdot \mathbf{J}_{\rm p}(t')dt',$$

where $\mathbf{J}_{\rm p}(t')$ is the expectation value of the paramagnetic current operator $\hat{\mathbf{J}}_{\rm p}$ computed with the wave function from the auxiliary Hamiltonian $\hat{H}_{\rm s}(t')$ at time t'. This vector potential corresponds to the mean-field contribution from the transverse photon modes, and the $t \to -\infty$ can be replaced by the appropriate initial conditions that solve the mode-resolved Maxwell equation. We note that if we keep the (discretized) continuum of modes, we can also describe the radiative dissipation (openness) of a photonic environment from first principles [17,23].

To define the exchange-correlation potential of KS QEDFT, we can use the local-force equation [32,33], which avoids the differentiability issue for energy functionals, the causality issue for action functionals in the time-dependent cases, and the numerical cost of the OEP procedure of orbital-dependent functionals. The local-force equation can be obtained from the equation of motion (EOM) of the paramagnetic current density $\hat{\mathbf{j}}_{\rm p}(\mathbf{r}) = \frac{1}{2i}\sum_{l=1}^{N_e}(\delta(\mathbf{r}-\mathbf{r}_l)\overrightarrow{\nabla}_l - \overleftarrow{\nabla}_l\delta(\mathbf{r}-\mathbf{r}_l))$. For ground-state (static) wave functions, the local-force equation for the PF Hamiltonian is

$$\rho(\mathbf{r})\nabla v_{\rm ext}(\mathbf{r}) = \langle\hat{\mathbf{F}}_T(\mathbf{r})\rangle_\Psi + \langle\hat{\mathbf{F}}_W(\mathbf{r})\rangle_\Psi - \frac{1}{c}\langle(\hat{\tilde{\mathbf{A}}}\cdot\nabla)\hat{\mathbf{j}}_{\rm p}(\mathbf{r})\rangle_\Psi, \quad (4)$$

where $\rho(\mathbf{r})$ is the electron density of the coupled light-matter ground state $|\Psi\rangle$, $\hat{\mathbf{F}}_T(\mathbf{r}) = \frac{i}{2}[\hat{\mathbf{j}}_{\rm p}(\mathbf{r}), \sum_{l=1}^{N_e}\nabla_l^2]$ the kinetic-force density, and $\hat{\mathbf{F}}_W(\mathbf{r}) = -\frac{i}{2}[\hat{\mathbf{j}}_{\rm p}(\mathbf{r}), \sum_{l\neq k}^{N_e} w(\mathbf{r}_l, \mathbf{r}_k)]$ the interaction-force density. Here the expectation value $\langle\ldots\rangle$ is evaluated at the exact ground state $|\Psi\rangle$ of the PF Hamiltonian. Similarly, we can find the local-force equation for the auxiliary Hamiltonian [Eq. (3)]

$$\rho_{\rm s}(\mathbf{r})\nabla v_{\rm s}(\mathbf{r}) = \langle\hat{\mathbf{F}}_T(\mathbf{r})\rangle_\Phi - \frac{1}{c}(\tilde{\mathbf{A}}_{\rm s}\cdot\nabla)\langle\hat{\mathbf{j}}_{\rm p}(\mathbf{r})\rangle_\Phi, \quad (5)$$

where $|\Phi\rangle$ is a Slater determinant for the ground state of the noninteracting auxiliary Hamiltonian $\hat{H}_{\rm s}$ and $\rho_{\rm s}(\mathbf{r})$ is the corresponding ground-state density.

If we now assume that both the PF and the auxiliary Hamiltonian have the same ground-state density $\rho(\mathbf{r}) = \rho_{\rm s}(\mathbf{r})$, the difference between the two local-force equations [Eqs. (4) and (5)] defines the mean-field exchange-correlation (Mxc) potential $v_{\rm Mxc}(\mathbf{r}) = v_{\rm s}(\mathbf{r}) - v_{\rm ext}(\mathbf{r})$ as

$$\rho(\mathbf{r})\nabla v_{\rm Mxc}(\mathbf{r}) = \langle\hat{\mathbf{F}}_T(\mathbf{r})\rangle_\Phi - \langle\hat{\mathbf{F}}_T(\mathbf{r})\rangle_\Psi - \langle\hat{\mathbf{F}}_W(\mathbf{r})\rangle_\Psi + \frac{1}{c}\langle(\hat{\tilde{\mathbf{A}}}\cdot\nabla)\hat{\mathbf{j}}_{\rm p}(\mathbf{r})\rangle_\Psi - \frac{1}{c}(\tilde{\mathbf{A}}_{\rm s}\cdot\nabla)\langle\hat{\mathbf{j}}_{\rm p}(\mathbf{r})\rangle_\Phi. \quad (6)$$

For the ground-state (or static) scenarios, the constant classical vector potential $\tilde{\mathbf{A}}_{\rm s}$ in the auxiliary Hamiltonian (3) can be eliminated through a gauge transformation on the ground-state wave function. This operation removes the last term in Eq. (6). To restore also the vector potential (photon density) of the original system, we need to include an exchange-correlation current in the Maxwell equation for the vector potential and solve it with the auxiliary system in a self-consistent way [27]. However, the vector potential becomes most relevant for beyond-dipole or time-dependent situations and will hence be investigated in dedicated manuscripts. Equation (6) allows us to define the electron-electron and electron-photon exchange-correlation potentials. For instance, the Hartree-exchange potential $v_{\rm Hx}(\mathbf{r})$ for the (longitudinal) electron-electron interaction can be defined as [32,33]

$$\nabla^2 v_{\rm Hx}(\mathbf{r}) = -\nabla\cdot\left[\frac{\langle\hat{\mathbf{F}}_W(\mathbf{r})\rangle_\Phi}{\rho(\mathbf{r})}\right], \quad (7)$$

where we replace the the exact ground-state wave function $|\Psi\rangle$ with the Slater determinant $|\Phi\rangle$. For the electron-photon interaction, we define the electron-photon exchange-correlation (pxc) potential $v_{\rm pxc}(\mathbf{r})$ as

$$\nabla^2 v_{\rm pxc}(\mathbf{r}) = \frac{1}{c}\nabla\cdot\left[\frac{\langle(\hat{\tilde{\mathbf{A}}}\cdot\nabla)\hat{\mathbf{j}}_{\rm p}(\mathbf{r})\rangle_\Psi}{\rho(\mathbf{r})}\right], \quad (8)$$

where we do not know, in general, the exact wave function $|\Psi\rangle$ to obtain the pxc potential. Nevertheless, we can use a similar trick as for the Hartree-exchange potential to define the (transverse) electron-photon exchange potential from the light-matter interaction term $\frac{1}{c}\langle(\hat{\tilde{\mathbf{A}}}\cdot\nabla)\hat{\mathbf{j}}_{\rm p}(\mathbf{r})\rangle_\Psi$, together with the Breit-type approximation (9) introduced in Ref. [25] for the quantum fluctuations of the vector potential operator. This approximation for $\Delta\hat{\tilde{\mathbf{A}}} = \sum_{\alpha=1}^{M_p}\Delta\hat{\tilde{A}}_\alpha\tilde{\boldsymbol{\varepsilon}}_\alpha$, where $\Delta\hat{O} = \hat{O} - \langle\hat{O}\rangle$, is

$$\Delta\hat{\tilde{A}}_\alpha \approx -c\frac{\tilde{\lambda}_\alpha^2}{\tilde{\omega}_\alpha^2}\tilde{\boldsymbol{\varepsilon}}_\alpha\cdot\Delta\hat{\mathbf{J}}_{\rm p}. \quad (9)$$

We can then construct the px potential $v_{\rm px}(\mathbf{r})$ from

$$\begin{aligned}\frac{1}{c}\langle(\hat{\tilde{\mathbf{A}}}\cdot\nabla)\hat{\mathbf{j}}_{\rm p}(\mathbf{r})\rangle_\Psi &= \frac{1}{c}\langle[(\langle\hat{\tilde{\mathbf{A}}}\rangle_\Psi + \Delta\hat{\tilde{\mathbf{A}}})\cdot\nabla]\hat{\mathbf{j}}_{\rm p}(\mathbf{r})\rangle_\Psi \\ &\to \frac{1}{2c}\left\langle\left[\left(\tilde{\mathbf{A}}_{\rm s} + \sum_{\alpha=1}^{M_p}\frac{-c\tilde{\lambda}_\alpha^2}{\tilde{\omega}_\alpha^2}(\tilde{\boldsymbol{\varepsilon}}_\alpha\cdot\Delta\hat{\mathbf{J}}_{\rm p})\tilde{\boldsymbol{\varepsilon}}_\alpha\right)\cdot\nabla\right]\hat{\mathbf{j}}_{\rm p}(\mathbf{r})\right\rangle_\Phi \\ &\quad + \text{c.c.} \\ &= -\frac{1}{2}\sum_{\alpha=1}^{M_p}\frac{\tilde{\lambda}_\alpha^2}{\tilde{\omega}_\alpha^2}[\langle(\tilde{\boldsymbol{\varepsilon}}_\alpha\cdot\hat{\mathbf{J}}_{\rm p})(\tilde{\boldsymbol{\varepsilon}}_\alpha\cdot\nabla)\hat{\mathbf{j}}_{\rm p}(\mathbf{r})\rangle_\Phi + \text{c.c.}],\end{aligned}$$

where we use $\hat{\tilde{\mathbf{A}}} = \langle\hat{\tilde{\mathbf{A}}}\rangle_\Psi + \Delta\hat{\mathbf{A}}$. In the above relation we have replaced the mean-field vector potential $\langle\hat{\tilde{\mathbf{A}}}\rangle_\Psi$ with the auxiliary classical vector potential $\tilde{\mathbf{A}}_\mathrm{s}$ [Eq. (3)] and employed the Breit-type approximation for $\Delta\hat{\mathbf{A}}$ [Eq. (9)]. Since it is then not guaranteed anymore that this gives a real number, it is necessary to take only the real part of the expression with c.c. meaning the complex conjugate. Note that, in general, $\langle\hat{\tilde{\mathbf{A}}}\rangle_\Psi \neq \tilde{\mathbf{A}}_\mathrm{s}$, which could be controlled with an exchange-correlation current [27,28]. Alternatively, we can perform a gauge transformation such that $\langle\hat{\tilde{\mathbf{A}}}\rangle_\Psi = \tilde{\mathbf{A}}_\mathrm{s}$ and we obtain in this way also the full knowledge of the photonic part. In the last line, the classical vector potential $\tilde{\mathbf{A}}_\mathrm{s}$ and the contribution from the mean-field paramagnetic current $\mathbf{J}_\mathrm{p} = \langle\hat{\mathbf{J}}_\mathrm{p}\rangle_\Phi$ cancel each other. We thus define the electron-photon exchange potential $v_\mathrm{px}(\mathbf{r})$ as

$$\nabla^2 v_\mathrm{px}(\mathbf{r}) = -\nabla\cdot\left[\sum_{\alpha=1}^{M_p}\frac{\tilde{\lambda}_\alpha^2}{2\tilde{\omega}_\alpha^2}\frac{(\tilde{\boldsymbol{\varepsilon}}_\alpha\cdot\nabla)[\mathbf{f}_{\alpha,\mathrm{px}}(\mathbf{r})+\mathrm{c.c.}]}{\rho(\mathbf{r})}\right], \tag{10}$$

where

$$\mathbf{f}_{\alpha,\mathrm{px}}(\mathbf{r}) = \langle(\tilde{\boldsymbol{\varepsilon}}_\alpha\cdot\hat{\mathbf{J}}_\mathrm{p})\hat{\mathbf{j}}_\mathrm{p}(\mathbf{r})\rangle_\Phi. \tag{11}$$

Next, the electron-photon correlation (pc) potential $v_\mathrm{pc}(\mathbf{r})$ is defined as $v_\mathrm{pc}(\mathbf{r}) = v_\mathrm{pxc}(\mathbf{r}) - v_\mathrm{px}(\mathbf{r})$ and can be solved, if the exact wave function $|\Psi\rangle$ is known, using

$$\nabla^2 v_\mathrm{pc}(\mathbf{r}) = \frac{1}{c}\nabla\cdot\left[\frac{\langle(\hat{\tilde{\mathbf{A}}}\cdot\nabla)\hat{\mathbf{j}}_\mathrm{p}(\mathbf{r})\rangle_\Psi}{\rho(\mathbf{r})}\right] - \nabla^2 v_\mathrm{px}(\mathbf{r}),$$

which is obtained from the difference between Eqs. (8) and (10). The remaining correlation potential from both the electron-electron and electron-photon interaction, denoted as $v_\mathrm{c}(\mathbf{r})$, is defined as $v_\mathrm{Mxc}(\mathbf{r}) - v_\mathrm{Hx}(\mathbf{r}) - v_\mathrm{pxc}(\mathbf{r})$ and can, in principle, be obtained from Eqs. (6)–(8) as

$$\nabla^2 v_\mathrm{c}(\mathbf{r}) = \nabla\cdot\left[\frac{\langle\hat{\mathbf{F}}_T(\mathbf{r})\rangle_\Phi - \langle\hat{\mathbf{F}}_T(\mathbf{r})\rangle_\Psi + \langle\hat{\mathbf{F}}_W(\mathbf{r})\rangle_\Phi - \langle\hat{\mathbf{F}}_W(\mathbf{r})\rangle_\Psi}{\rho(\mathbf{r})}\right]. \tag{12}$$

Note that, in principle, we also have an equation of motion for the photonic part of the coupled system [27,28]. However, in the static long-wavelength case this equation becomes equivalent to $\langle\hat{\tilde{\mathbf{A}}}\rangle_\Psi = \tilde{\mathbf{A}}_\mathrm{s}$. For a fixed gauge in the physical as well as auxiliary KS system this can be achieved via an exchange-correlation current. This auxiliary current can become important to model more involved photonic observables and in the time-dependent case. Nevertheless, the photon-exchange approximation provides already access to information of the photon field as discussed Ref. [25]. A detailed discussion of the photonic aspects is beyond the scope of this work.

After defining the exchange-correlation potentials, we notice that the formulas for the Hartree-exchange, electron-photon exchange, and correlation potentials all have the form of the Poisson equation, which can be solved numerically:

$$\nabla^2 v(\mathbf{r}) = \nabla\cdot\left(\frac{\mathbf{h}(\mathbf{r})}{\rho(\mathbf{r})}\right),$$

where $v(\mathbf{r})$ represents a potential and $\mathbf{h}(\mathbf{r})$ a vector-valued function. This approach has been implemented in the OCTOPUS code [34] to obtain the Hartree-exchange potential [33]. Similarly, the px potential $v_\mathrm{px}(\mathbf{r})$ can be obtained by solving the corresponding Poisson equation (10). For one-electron systems coupled to one single dressed photon mode with the frequency $\tilde{\omega}$, light-matter coupling $\tilde{\lambda}$, and polarization direction $\tilde{\boldsymbol{\varepsilon}}$, the px potential $v_\mathrm{px}(\mathbf{r})$ can be obtained directly from the electron density (for details see Appendix B) using

$$v_\mathrm{px}(\mathbf{r}) = \frac{\tilde{\lambda}^2}{2\tilde{\omega}^2}\frac{(\tilde{\boldsymbol{\varepsilon}}\cdot\nabla)^2\rho^{\frac{1}{2}}(\mathbf{r})}{\rho^{\frac{1}{2}}(\mathbf{r})}. \tag{13}$$

In the homogeneous density limit, which leads to the local-density approximation (LDA), the expectation value in Eq. (11) can be evaluated in terms of a Slater determinant of plane waves and leads to [25]

$$\mathbf{f}_{\alpha,\mathrm{px}}(\mathbf{r}) \to \mathbf{f}_{\alpha,\mathrm{pxLDA}}(\mathbf{r}) = \frac{2V_d}{(2\pi)^d}\frac{k_\mathrm{F}^{d+2}(\mathbf{r})}{d+2}\tilde{\boldsymbol{\varepsilon}}_\alpha, \tag{14}$$

where $k_\mathrm{F}(\mathbf{r}) = 2\pi[\rho(\mathbf{r})/2V_d]^{1/d}$ and V_d is the volume of the d-dimensional unit sphere (i.e., $V_1 = 2$, $V_2 = \pi$, and $V_3 = 4\pi/3$). It can be shown that the force $\mathbf{f}_{\alpha,\mathrm{px}}(\mathbf{r})$ satisfies the zero-force condition [see Eq. (C2) in Appendix C]. The px potential within the homogeneous limit then becomes an explicit density functional and can be calculated by solving

$$\nabla^2 v_\mathrm{pxLDA}(\mathbf{r}) = -\sum_{\alpha=1}^{M_p}\frac{2\pi^2\tilde{\lambda}_\alpha^2}{\tilde{\omega}_\alpha^2}\left[(\tilde{\boldsymbol{\varepsilon}}_\alpha\cdot\nabla)^2\left(\frac{\rho(\mathbf{r})}{2V_d}\right)^{\frac{2}{d}}\right]. \tag{15}$$

In one dimension and for isotropic problems, the pxLDA potential has an explicit form, respectively,

$$v_\mathrm{pxLDA}(x) = -\frac{\pi^2}{8}\sum_{\alpha=1}^{M_p}\frac{\tilde{\lambda}_\alpha^2}{\tilde{\omega}_\alpha^2}\rho^2(x),$$

$$v_\mathrm{pxLDA}^\mathrm{iso}(\mathbf{r}) = -\frac{2\pi^2}{d}\sum_{\alpha=1}^{M_p}\frac{\tilde{\lambda}_\alpha^2}{\tilde{\omega}_\alpha^2}\left(\frac{\rho(\mathbf{r})}{2V_d}\right)^{\frac{2}{d}}.$$

For two and three dimensions one needs to solve the Poisson equation [Eq. (15)], using either the conjugate gradient or the Poisson-kernel method [34]. Yet, the correlation potential $v_\mathrm{c}(\mathbf{r})$ remains unknown in general, as it depends on the exact ground-state wave function [Eq. (12)], necessitating the use of alternative numerical methods like quantum Monte Carlo [35,36]. Nevertheless, we introduce a method in Sec. II C to explore one aspect of the correlation potential, namely, the electron-photon correlation potential, in the context of weak coupling in the light-matter interaction.

After obtaining the px potential from the local-force equation, we explore the associated px energy below. We note that when employing Eq. (9) in the PF Hamiltonian [Eq. (2)], we need to consistently also take the contribution of the photonic energy into account [25]. That is, the replacement of the photonic operator with the paramagnetic current operator in the last term of Eq. (2) gives a counteracting contribution to

the light-matter interaction term $\hat{\mathbf{A}} \cdot \hat{\mathbf{J}}_\mathrm{p}$. A comparison with the EOM of a correspondingly defined Breit-type Hamiltonian [25] reveals that the substitution leads to

$$\frac{1}{c}\langle \hat{\mathbf{A}} \cdot \hat{\mathbf{J}}_\mathrm{p} \rangle_\Psi + \sum_{\alpha=1}^{M_p} \tilde{\omega}_\alpha \langle \hat{\bar{a}}_\alpha^\dagger \hat{\bar{a}}_\alpha \rangle_\Psi \to E_\mathrm{px}[\rho],$$

where the electron-photon exchange energy is defined as

$$E_\mathrm{px}[\rho] = -\sum_{\alpha=1}^{M_p} \frac{\tilde{\lambda}_\alpha^2}{2\tilde{\omega}_\alpha^2} \langle (\tilde{\boldsymbol{\varepsilon}}_\alpha \cdot \hat{\mathbf{J}}_\mathrm{p})\Phi[\rho] | (\tilde{\boldsymbol{\varepsilon}}_\alpha \cdot \hat{\mathbf{J}}_\mathrm{p})\Phi[\rho] \rangle. \quad (16)$$

Here the factor of $\frac{1}{2}$ results from the counteracting photonic energy contribution. In the homogeneous limit, the px energy becomes (for details see Appendix C)

$$E_\mathrm{pxLDA}[\rho] = \frac{-2\pi^2}{(d+2)(2V_d)^{\frac{2}{d}}} \sum_{\alpha=1}^{M_p} \frac{\tilde{\lambda}_\alpha^2}{\tilde{\omega}_\alpha^2} \int d\mathbf{r}\, \rho^{\frac{2+d}{d}}(\mathbf{r}). \quad (17)$$

This form can be derived either through applying the LDA on the energy functional of Eq. (16) or via the exchange virial relation using the LDA for the force from Eq. (14) (see Appendix C for details). We note that the exchange force, which in general has transverse components, needs to be taken into account to fulfill the exchange virial relation [33]. When determining the pxLDA potential from the functional derivative of the pxLDA energy [Eq. (17)], we end up with the isotropic pxLDA potential $v_\mathrm{pxLDA}^\mathrm{iso}(\mathbf{r})$. However, this isotropic potential lacks information about the polarization of photon modes. To preserve this information, it is essential to use the pxLDA potential obtained from the local-force equation in the KS equations and subsequently compute the pxLDA energy after obtaining the electron density. Nevertheless, reproducing the total energy of the original system in our approach requires the inclusion and tracking of the vector potential (photon density), which is eliminated by the gauge chosen during the construction of the auxiliary system. Benchmarking the total energy from our approach is planned for future work.

In practice, the KS Hamiltonian, which is designed to reproduce the electron density of the PF Hamiltonian [Eq. (2)], has to be solved in a self-consistent way for ground-state calculations similar to standard density functional theory (DFT) [37,38]:

(1) Calculate the Mxc potential $v_\mathrm{Mxc}(\mathbf{r})$ using either the KS orbitals or the electron density.

(2) Construct the KS Hamiltonian $\hat{H}_\mathrm{KS}$ using the Hamiltonian of Eq. (3) with $v_\mathrm{KS}(\mathbf{r}) = v_\mathrm{ext}(\mathbf{r}) + v_\mathrm{Mxc}(\mathbf{r})$ and without the vector potential in the time-independent cases.

(3) Solve the resulting KS Hamiltonian and obtain the KS orbitals and electron density, which are used in step 1 to get the associated Mxc potentials.

(4) Loop through steps 1 to 3 until the electron density converges within a desired threshold.

For time-dependent calculations, once the ground state of the KS Hamiltonian $|\Phi_\mathrm{KS}\rangle$ is obtained, the time propagation of the ground state is determined by solving the nonlinear Schrödinger-type evolution equation $i\partial_t|\Phi_\mathrm{KS}(t)\rangle = \hat{H}_\mathrm{KS}(t)|\Phi_\mathrm{KS}(t)\rangle$ with the time-dependent Hamiltonian from Eq. (3), together with the auxiliary classical vector potential $\tilde{\mathbf{A}}_\mathrm{s}(t)$, and replacing $v_\mathrm{s}(\mathbf{r},t) \to v_\mathrm{KS}(\mathbf{r},t)$ [1,19,39,40]. Note that the Mxc potential based on the local-force equation of Eq. (6) is strictly speaking *only* for the static case, making it an adiabatic approximation when used in time-dependent simulations. Although it is possible to derive nonadiabatic potentials (see Refs. [25,32,33] for details), this is beyond the scope of our paper. Below we thus use the adiabatic approximation to obtain associated spectra [39,40]. When it comes to observables beyond the density and the ground-state energy of the original system, the KS method offers no straightforward way on how to achieve them. Nevertheless, as in standard (time-dependent) DFT, the theorems of QEDFT [1,27] show that in principle all observables can be determined. The task of finding valid approaches to other quantities, like entanglement entropy between light and matter [41], poses a challenge that goes beyond the scope of our work.

C. Weak-coupling limit: Perturbation-theory analysis

The px potential has been derived from the PF Hamiltonian using the photon-coupled homogeneous electron-gas basis [25,42]. In the limit $\lambda_\alpha \to \infty$ and $\omega_\alpha \to \infty$, the px potential becomes the sole contribution. While it vanishes for $\lambda_\alpha \to 0$ (as it should), its behavior in this limit has not been extensively studied. For simplicity, we focus on one effective mode [26], as simulations with numerous modes pose numerical challenges for exact reference calculations. This is the focus of this section. However, the explored approximate electron-photon functionals can be easily extended to accommodate any number of photon modes without significant numerical overhead.

To better understand the applicability of the px and pxLDA approximations for the PF Hamiltonian, we compare it with static perturbation theory. Our starting Hamiltonian with one dressed photon mode, i.e., Eq. (2) with one mode, is rewritten as

$$\hat{H}_\mathrm{PF} = \hat{H}_\mathrm{M} + \frac{1}{c}\hat{\mathbf{A}} \cdot \hat{\mathbf{J}}_\mathrm{p} + \hat{H}_\gamma, \quad (18)$$

where the Hamiltonian for the matter subsystem is

$$\hat{H}_\mathrm{M} = -\frac{1}{2}\sum_{l=1}^{N_e} \nabla_l^2 + \sum_{l=1}^{N_e} v_\mathrm{ext}(\mathbf{r}_l) + \frac{1}{2}\sum_{l\neq k}^{N_e} w(\mathbf{r}_l, \mathbf{r}_k), \quad (19)$$

and the Hamiltonian for the dressed photon mode is

$$\hat{H}_\gamma = \tilde{\omega}\left(\hat{\bar{a}}^\dagger \hat{\bar{a}} + \frac{1}{2}\right).$$

In this section we overload the notation $\hat{H}_\mathrm{PF}$ for one photon mode [26], compared to Eq. (2). If we mention one-mode cases, we refer to Eq. (18); otherwise, we refer to the more general multimode form of Eq. (2).

We denote $\hat{H}_\mathrm{M}|m^{(0)}\rangle = \epsilon_m^{(0)}|m^{(0)}\rangle$, where $\epsilon_m^{(0)}$ is the energy for the mth unperturbed many-body matter state $|m^{(0)}\rangle$. Furthermore, we have $\hat{H}_\gamma|\tilde{n}\rangle = \tilde{\omega}(\tilde{n}+1/2)|\tilde{n}\rangle$, where $\tilde{\omega}$ and $\tilde{n}$ are the dressed photon frequency and photon number for the photon mode $|\tilde{n}\rangle$, respectively. The vector potential for

the dressed cavity is $\hat{\tilde{\mathbf{A}}} = \hat{\tilde{A}}\tilde{\boldsymbol{\epsilon}} = (c\tilde{\lambda}/\sqrt{2\tilde{\omega}})(\hat{\tilde{a}}^\dagger + \hat{\tilde{a}})$, where $\tilde{\lambda} = \lambda$ and $\tilde{\omega}^2 = \omega^2 + N_e\lambda^2$ (see Appendix A). Next, we assume weak light-matter coupling such that the light-matter interaction can be considered as a perturbation to the matter Hamiltonian [Eq. (19)],

$$\Delta\hat{V} = \frac{1}{c}\hat{\tilde{\mathbf{A}}}\cdot\hat{\mathbf{J}}_\mathrm{p} = \frac{\tilde{\lambda}}{\sqrt{2\tilde{\omega}}}(\hat{\tilde{a}}^\dagger + \hat{\tilde{a}})(\tilde{\boldsymbol{\epsilon}}\cdot\hat{\mathbf{J}}_\mathrm{p}).$$

The unperturbed system is the composite system that consists of the ground state of the matter $|0^{(0)}\rangle$ and that of the one-dressed-photon-mode subsystem $|\tilde{0}\rangle$. We write the ground state of the unperturbed composite system as a direct tensor product state $|\Psi_0^{(0)}\rangle = |0\tilde{0}\rangle = |0^{(0)}\rangle \otimes |\tilde{0}\rangle$.

In the weak light-matter coupling regime, the modified ground-state wave function $|\Psi_0\rangle$ up to the first-order correction is

$$|\Psi_0\rangle \approx \left|\Psi_0^{(0)}\right\rangle + \left|\Psi_0^{(1)}\right\rangle,$$

where $|\Psi_0^{(1)}\rangle$ is the first-order correction to the ground-state wave function, which only involves the contribution from the first photon sector $|\tilde{1}\rangle$,

$$\left|\Psi_0^{(1)}\right\rangle = -\frac{\tilde{\lambda}}{\sqrt{2}\tilde{\omega}^{3/2}}\sum_{m=0}^{\infty}\frac{\langle m^{(0)}|(\tilde{\boldsymbol{\epsilon}}\cdot\hat{\mathbf{J}}_\mathrm{p})|0^{(0)}\rangle}{1+\Delta\epsilon_{m0}^{(0)}/\tilde{\omega}}|m\tilde{1}\rangle,$$

where $\Delta\epsilon_{m0}^{(0)} = \epsilon_m^{(0)} - \epsilon_0^{(0)}$ and $|m\tilde{1}\rangle = |m^{(0)}\rangle \otimes |\tilde{1}\rangle$. The modified ground-state wave function is an entangled state, which cannot be rewritten as a single tensor product state of the matter and photonic state.

Using the modified ground-state wave function $|\Psi_0\rangle$ and Eq. (8), we evaluate the pxc potential up to the lowest order of the light-matter coupling,

$$\begin{aligned}\nabla^2 v_\mathrm{pxc}(\mathbf{r}) &\approx \frac{1}{c}\boldsymbol{\nabla}\cdot\left[\frac{\left\langle\Psi_0^{(1)}\right|(\hat{\tilde{\mathbf{A}}}\cdot\boldsymbol{\nabla})\hat{\mathbf{j}}_\mathrm{p}(\mathbf{r})\left|\Psi_0^{(0)}\right\rangle}{\rho(\mathbf{r})}\right] + \mathrm{c.c.} = \boldsymbol{\nabla}\cdot\left[\frac{-\tilde{\lambda}^2}{2\tilde{\omega}^2\rho(\mathbf{r})}\sum_{m=0}^{\infty}\frac{\langle 0^{(0)}|\tilde{\boldsymbol{\epsilon}}\cdot\hat{\mathbf{J}}_\mathrm{p}|m^{(0)}\rangle\langle m^{(0)}|\tilde{\boldsymbol{\epsilon}}\cdot\boldsymbol{\nabla}\hat{\mathbf{j}}_\mathrm{p}(\mathbf{r})|0^{(0)}\rangle}{1+\Delta\epsilon_{m0}^{(0)}/\tilde{\omega}}\right] + \mathrm{c.c.}\\ &= -\boldsymbol{\nabla}\cdot\left[\frac{\tilde{\lambda}^2}{2\tilde{\omega}^2}\frac{\langle(\tilde{\boldsymbol{\epsilon}}\cdot\hat{\mathbf{J}}_\mathrm{p})(\tilde{\boldsymbol{\epsilon}}\cdot\boldsymbol{\nabla})\hat{\mathbf{j}}_\mathrm{p}(\mathbf{r})\rangle_{\Psi_0^{(0)}}}{\rho(\mathbf{r})}\right] + \boldsymbol{\nabla}\cdot\left[\frac{\tilde{\lambda}^2}{2\tilde{\omega}^2\rho(\mathbf{r})}\sum_{m=1}^{\infty}\frac{\langle 0^{(0)}|\tilde{\boldsymbol{\epsilon}}\cdot\hat{\mathbf{J}}_\mathrm{p}|m^{(0)}\rangle\langle m^{(0)}|\tilde{\boldsymbol{\epsilon}}\cdot\boldsymbol{\nabla}\hat{\mathbf{j}}_\mathrm{p}(\mathbf{r})|0^{(0)}\rangle}{1+\tilde{\omega}/\Delta\epsilon_{m0}^{(0)}}\right] + \mathrm{c.c.},\end{aligned}$$

where we have only the contribution between $|\Psi_0^{(0)}\rangle$ and $|\Psi_0^{(1)}\rangle$ due to the orthogonality of the photonic states. In the last line we separate a px-like contribution, where we use $|\Psi_0^{(0)}\rangle$ instead of $|\Phi\rangle$ in Eq. (11), from the pxc potential with the help of the identity $\mathbb{1} = \sum_{m=0}^{\infty}|m^{(0)}\rangle\langle m^{(0)}|$. Then, the pc potential in the weak-coupling regime is

$$\nabla^2 v_\mathrm{pc}(\mathbf{r}) \approx \boldsymbol{\nabla}\cdot\left[\frac{\tilde{\lambda}^2}{2\tilde{\omega}^2\rho(\mathbf{r})}\sum_{m=1}^{\infty}\frac{\langle 0^{(0)}|\tilde{\boldsymbol{\epsilon}}\cdot\hat{\mathbf{J}}_\mathrm{p}|m^{(0)}\rangle\langle m^{(0)}|\tilde{\boldsymbol{\epsilon}}\cdot\boldsymbol{\nabla}\hat{\mathbf{j}}_\mathrm{p}(\mathbf{r})|0^{(0)}\rangle}{1+\tilde{\omega}/\Delta\epsilon_{m0}^{(0)}}\right] + \mathrm{c.c.} \tag{20}$$

When $\tilde{\omega}\to\infty$ (i.e., in the strong-coupling regime or large photon frequency regime), the pc potential vanishes, and the pxc becomes a px-like potential, consistent with the results obtained from the analysis of the photon-coupled homogeneous electron-gas basis [25].

Computing the pc potential in the weak coupling [Eq. (20)] requires all the information of the many-body matter states, which poses numerical challenges. Alternatively, the light-matter interaction in the weak-coupling regime can be accurately obtained using the OEP approach [22,23]. Instead of solving Eq. (20), we here propose the following formula with a correlation factor ξ_c to approximate the pc potential in the weak-coupling regime for one photon mode,[2]

$$\nabla^2 v_\mathrm{pc}(\mathbf{r}) \approx \xi_c\boldsymbol{\nabla}\cdot\left[\frac{\tilde{\lambda}^2}{2\tilde{\omega}^2}\frac{\langle(\tilde{\boldsymbol{\epsilon}}\cdot\hat{\mathbf{J}}_\mathrm{p})(\tilde{\boldsymbol{\epsilon}}\cdot\boldsymbol{\nabla})\hat{\mathbf{j}}_\mathrm{p}(\mathbf{r})\rangle_{\Psi_0^{(0)}} + \mathrm{c.c.}}{\rho(\mathbf{r})}\right].$$

This formula is obtained by assuming $\Delta\epsilon_{m0}^{(0)} \gg \tilde{\omega}$ in the second line of Eq. (20) such that the dependence of the denominator on the index m can be neglected. The (positive) correlation factor ξ_c depends on the light-matter coupling and photon frequency, and vanishes when $\tilde{\omega}\to\infty$, i.e., in the strong-coupling or large photon frequency regime. Thus, we use the following formula for the pxc potential when exploring the weak-coupling regime:

$$\nabla^2 v_\mathrm{pxc}(\mathbf{r}) \approx -\eta_\mathrm{c}\boldsymbol{\nabla}\cdot\left[\frac{\tilde{\lambda}^2}{2\tilde{\omega}^2}\frac{\langle(\tilde{\boldsymbol{\epsilon}}\cdot\hat{\mathbf{J}}_\mathrm{p})(\tilde{\boldsymbol{\epsilon}}\cdot\boldsymbol{\nabla})\hat{\mathbf{j}}_\mathrm{p}(\mathbf{r})\rangle_\Phi + \mathrm{c.c.}}{\rho(\mathbf{r})}\right],$$

where we replace $|\Psi_0^{(0)}\rangle$ with $|\Phi\rangle$ and use Eq. (10), and we define a renormalization factor $\eta_\mathrm{c} = 1 - \xi_\mathrm{c}$ for the px potential to take the electron-photon correlation contribution into account. We denote this formula as the η_c-px approach here and below. The renormalization factor η_c is determined by perturbation theory, e.g., comparing the results with the exact or OEP approach. Hereafter, we apply the approximated pxc potential to various one-electron systems. It is anticipated that the outcomes may differ from the exact results, as the correlation potential from the kinetic- and interaction-force density [Eq. (12)], and the electron-photon correlation potential arising from employing the Slater determinant in the pxc potential instead of the exact wave function, are neglected. Below we determine the renormalization factor by comparing it with the electron density obtained from the exact (or OEP) approach.

[2]For multimode cases, each photon mode has its correlation factor $\xi_{c,\alpha}$. The correlation factor $\xi_{c,\alpha} = \xi_{c,\alpha}(\{\lambda_\alpha\},\{\omega_\alpha\})$ for each photon mode α is a function of the light-matter coupling as well as the photon frequency.

This factor relies on the electron-photon correlation potential, which is based on the (unknown) exact wave function. This process resembles the construction of the electron-electron correlation potential in standard DFT [38], which is numerically determined and parametrized from the solution of the homogeneous electron gas using the quantum Monte Carlo method. However, systematically identifying and parametrizing the renormalization factor or electron-photon correlation potential poses another challenging numerical task [36].

III. RESULTS AND DISCUSSION

We analyze the performance of the different functionals derived in the previous section by applying them to three different one-electron systems coupled to an effective single mode of a perfect cavity, e.g., Fabry-Pérot cavity.[3] Specifically, we consider electron-photon interaction in a one-dimensional HO, a two-dimensional quantum ring, and a three-dimensional hydrogen atom. In one- and two-dimensional systems, we can directly solve the corresponding PF Hamiltonians using exact diagonalization, which serves as a benchmark for approximate QEDFT results. We focus the analysis and comparison on the electron density since this is the fundamental quantity of QEDFT in the long-wavelength limit. For the three-dimensional hydrogen atom, we examine the ground-state electron density by comparing the OEP approach to the px and pxLDA approximations. Additionally, for the hydrogen atom, we explore its optical absorption spectra through time-dependent QEDFT [1,18,19] (see Appendix D for all computational details). Although our main focus is on investigating the behavior of electron-photon interaction without complicating the study with (approximate) electron-electron interaction, in Appendix E we also present a He atom to showcase that the approach is directly applicable to multielectron problems.

A. Harmonic oscillator coupled to a photon mode

We first consider a one-dimensional HO with the external potential $v_{\mathrm{SHO}}(x) = x^2/2$ coupled to a photon mode (see the computational details in Appendix D). We explore both weak- and strong-coupling regimes by using two different light-matter couplings, $\lambda = 0.005$ and 4.0, along with two photon frequencies $\omega = 1.0$ and 5.1. Figure 1 shows the electron density differences between inside and outside the cavity, $\Delta\rho(x) = \rho_\lambda(x) - \rho_{\lambda=0}(x)$. Here and below, when we mention the outside-cavity case, we mean zero light-matter coupling, i.e., $\lambda = 0$. In the weak-coupling ($\lambda = 0.005$) and low-photon-frequency ($\omega = 1.0$, i.e., on resonance with the first excited state of the HO) scenario, both px and pxLDA approximations overestimate the effect of the mode on the electron density. Following the discussion in Sec. II C, we can rectify this by introducing the perturbation-based renormalization factor ($\eta_c = \frac{1}{4}$) for the px potential. In the weak-coupling but high-photon-frequency ($\omega_\alpha = 5.1$) case, the px functional slightly overestimates the electron density,

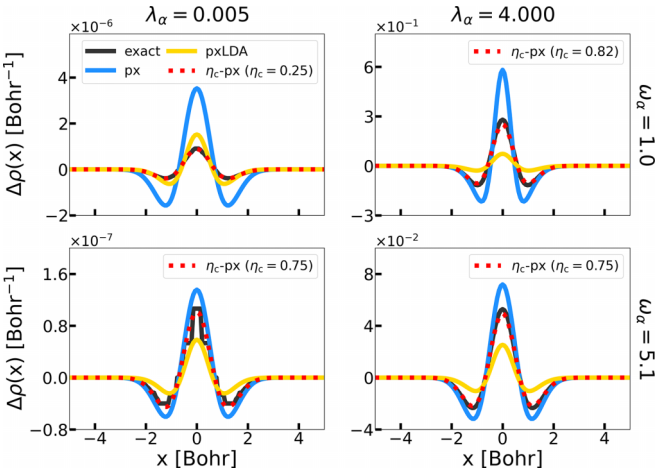

FIG. 1. Electron-density differences between the inside and outside cavity, $\Delta\rho(x) = \rho_\lambda(x) - \rho_{\lambda=0}(x)$, in the weak- and strong-coupling regimes. The results are computed via the exact diagonalization and different approximate QEDFT functionals.

while the pxLDA approximation slightly underestimates it. The η_c-px functional reproduces the exact result, and the η_c factor becomes close to 1.0.

In the strong-coupling regime ($\lambda = 4.0$ and $\lambda/\omega \geqslant 0.1$) both the px and pxLDA approximations exhibit small deviations from the exact electron density, similar to the scenario seen in the weak coupling but with a large photon frequency ($\lambda = 0.005$ and $\omega = 5.1$). The η_c-px functional can be used to restore the exact results, and the η_c factor approaches 1.0 in this context, implying that the electron-photon correlation becomes small. These numerical findings demonstrate yet again that both the px and pxLDA approximate functionals perform well in the strong-coupling regime. While the pxLDA functional tends to underestimate the effect of the cavity on the electron density compared to the px approximation, it captures the changes qualitatively correct for one-dimensional problems. The presented approximation strategy also gives an intuitive understanding of the effect of the cavity in the strong-coupling regime. Expressing the photon fluctuation operator via the current operator [Eq. (9)] leads to a renormalization of the electron mass (along the polarization direction), a feature that is also predicted for the homogeneous electron gas (HEG) coupled to an optical cavity [42]. Since this increases the effective mass of the electron, i.e., the kinetic contribution in the Schrödinger equation is decreased, the electron becomes more localized.

B. Quantum ring coupled to a photon mode

When the photon mode is in resonance with the first excited state of a quantum ring [$\Delta\epsilon^{(0)}_{10} = 0.125$ for a confining potential $v_{\mathrm{QR}}(\mathbf{r}) = \xi_1|\mathbf{r}|^2/2 + \xi_2 \exp(-|\mathbf{r}|^2/\xi_3^2)$, with $\xi_1 = 0.7827$, $\xi_2 = 17.7$, and $\xi_3 = 0.997$ [43]] in the weak-coupling regime, the electron density accumulates perpendicular to the polarization direction, which is set to x here, while in the strong-coupling regime, the density aligns along the polarization direction [see Fig. 2(a)] (for the computational details see Appendix D). This shift in behavior makes the quantum

[3]For single-cavity-mode cases, the px and pc potentials depend only on the ratio between the light-matter coupling and bare photon frequency, i.e., $\lambda_\alpha/\omega_\alpha$.

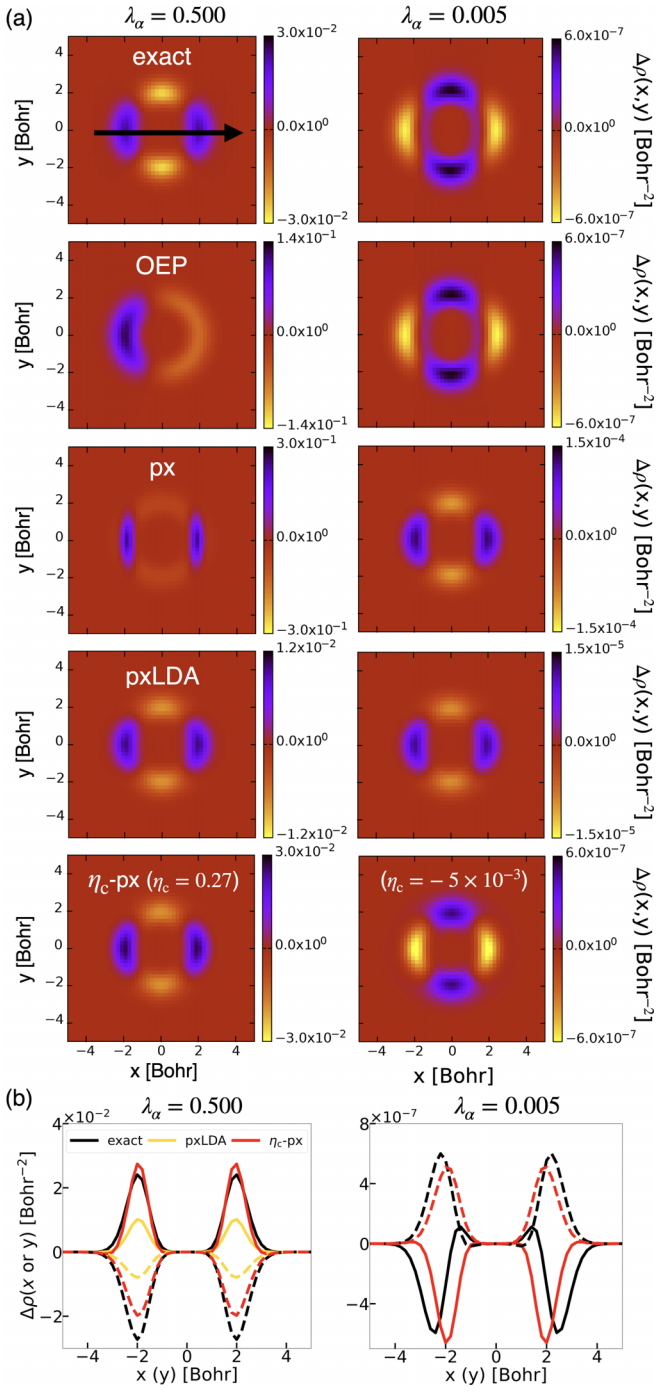

FIG. 2. The photon mode is polarized along the x direction (the solid right arrow) and has a frequency of $\omega = 0.125$, in resonance with the first excited state of the two-dimensional quantum ring. (a) The electron-density difference inside and outside the cavity for the exact and various approximate QEDFT functionals in both strong- and weak-coupling regimes. (b) The electron-density difference along the x (solid lines) and y (dashed lines) directions (the cut through the center of the quantum ring) in both strong- and weak-coupling scenarios. The renormalization factors η_c are 0.27 and -5×10^{-3} in the strong- and weak-coupling regime, respectively.

ring an excellent case to test if the approximate QEDFT functionals can reproduce the correct feature of the electron density from the weak- to strong-coupling regimes.

Figure 2(a) shows electron density differences within and outside the cavity under both strong- and weak-coupling conditions, considering the different approximate QEDFT functionals. In the strong-coupling regime ($\lambda = 0.5$), the OEP functional in exchange-approximation fails to qualitatively replicate the exact electron density [22], whereas the px functional, while providing a qualitative match, tends to overestimate the effect of the cavity. The pxLDA functional yields an improved agreement with the exact result in the strong-coupling regime. Additionally, we see that the η_c-px functional helps to recover quantitatively the exact results for this case. Figure 2(b) provides a comparison of electron-density differences along the x and y directions for the exact, pxLDA, and η_c-px methods. In the strong-coupling regime, the electron accumulates and behaves more classically along the polarization, similar to the one-dimensional HO case.

In the weak-coupling regime ($\lambda = 0.005$), neither the px nor the pxLDA approximations capture the desired feature [Fig. 2(a)]. In contrast, the η_c-px approach manages to capture the weak-coupling feature, even though small deviations still exist [Fig. 2(b)] due to the approximation we made for the η_c-px potential developed in Sec. II C and the neglect of other correlation potentials. These observations highlight the electron-photon correlation contribution in the weak-coupling regime. Conversely, in the strong-coupling regime, we can use approximate px potentials alone to capture the strong-coupling features because the pc potential quickly vanishes with $\tilde{\omega}_\alpha$ as discussed in Sec. II C.

C. Hydrogen atom coupled to a photon mode

We now turn our attention to a more realistic system, a hydrogen atom coupled to a photon mode (see Appendix D for the computational details). While this system might seem simple with one atom and one electron coupled to one photon mode, the exact diagonalization of the PF Hamiltonian in real space to obtain the electron density poses already computational challenges, demanding significant memory resources to converge the results with respect to the real-space grid size and the number of photon Fock states. As an alternative, we rely on the results obtained from the OEP functional in exchange approximation as our reference, especially, in the weak-coupling regime, where the OEP approach works well.

Figure 3(a) compares the electron-density difference between inside and outside the cavity, with a frequency that is in resonance with the first excited state of the bare hydrogen atom and the polarization along the x direction. We evaluate this using OEP, pxLDA, and η_c-px functionals. Similar to the HO case, both px and pxLDA approximations overestimate electron-density changes in the weak-coupling regime ($\lambda = 5 \times 10^{-5}$), with px results (not shown) an order of magnitude higher. Applying a renormalization factor $\eta_c = 0.1$ to px reproduces the OEP results. In the strong-coupling regime ($\lambda = 0.5$), we provide the OEP, px, and pxLDA results. Although OEP may not provide accurate results due to its perturbative nature in this regime, we anticipate that px and pxLDA offer upper and lower bounds for the electron-density difference based on our experience with the other test systems.

After analyzing the ground-state electron density, we proceed to compute the linear-response optical absorption

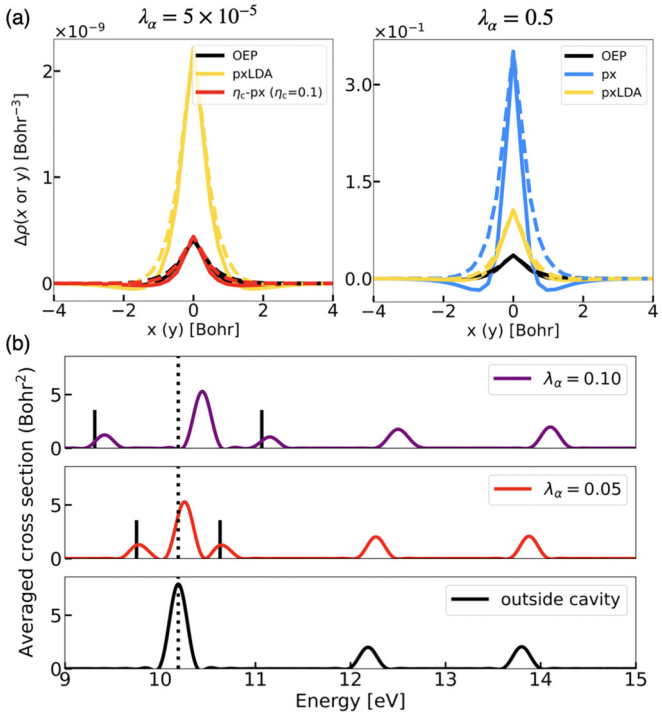

FIG. 3. The photon mode is polarized along the x direction and a photon frequency of 0.3745 hartree (10.19 eV), in resonance with the first excited state of the hydrogen atom. (a) The electron-density differences $\Delta\rho$ along the x (solid lines) and y (dashed lines) directions in the weak- and strong-coupling regimes, computed using various QEDFT approximations. (b) The optical spectrum of the hydrogen atom inside and outside of the cavity. The results for inside the cavity are obtained using the pxLDA functional. The dashed lines represent the photon frequency of the photon mode, while the vertical solid black lines in both inside-cavity cases are the eigenvalues from the JC model (please see the main text).

spectra for the hydrogen atom inside the cavity using the pxLDA functional. While the OEP functional in exchange approximation is suitable for weak-coupling spectra [23], exploring strong coupling with approximate QEDFT functionals for realistic materials remains uncharted territory. Figure 3(b) shows the optical absorption spectrum (or cross section) of the hydrogen atom interacting with a photon mode in the strong-coupling regime. The polarization is along the x direction, and the photon frequency is in resonance with the atom's first excitation, i.e., $\omega_\alpha = 0.3745$. Outside the cavity, the first peak corresponds to three dipole transitions: $1s \to 2p_x$, $1s \to 2p_y$, and $1s \to 2p_z$. These $2p$ orbitals have degenerate energy levels. However, inside the cavity with a light-matter coupling of $\lambda = 0.05$, part of the first peak splits into two peaks. These are the lower and upper polaritons arising from the hybridization between the $1s \to 2p_x$ transition and the photon mode. The other two transitions, $1s \to 2p_y$ and $1s \to 2p_z$, remain largely unchanged since the photon mode is polarized along the x direction. As the light-matter coupling increases from 0.05 to 0.1, the Rabi splitting between the lower and upper polariton doubles. Notably, other peak positions are also influenced, even when the photon mode is not in resonance with them.

Here we compare our QEDFT results with the widely used Jaynes-Cummings (JC) model, which describes light-matter coupled two-level systems well in the weak-coupling regime. The JC Hamiltonian within the *rotating-wave approximation*, describing a two-level system with energy difference ω_0 coupled to a photon mode with photon frequency ω and polarization $\boldsymbol{\varepsilon}$, is given by (in Hartree atomic units)

$$\hat{H}_{\rm JC} = \omega\hat{a}^\dagger\hat{a} + \omega_0\frac{\hat{\sigma}_z}{2} + g(\hat{a}\hat{\sigma}_+ + \hat{a}^\dagger\hat{\sigma}_-) + \frac{\omega_0}{2},$$

where $\hat{\sigma}_z$ is the Pauli matrix representing the two energy levels, $g = \lambda\sqrt{\omega/2}(\mathbf{d}\cdot\boldsymbol{\varepsilon})$,[4] where $\mathbf{d}$ is the dipole matrix element between the two levels, and the last term $(\omega_0/2)$ is used to reset the energy of the lowest state of the two levels system to zero. The polaritonic eigenvalues for the photon vacuum state $(n = 0)$ are given by $E_\pm(n = 0, \delta) = \frac{\omega+\omega_0}{2} \pm \frac{1}{2}\sqrt{4g^2 + \delta}$ where $\delta = \omega_0 - \omega$. For the $1s$ and $2p_x$ orbitals of the hydrogen atom coupled to a photon mode with $\delta = 0$, the polariton energies are $E_\pm(n = 0, \delta = 0) = \omega_0 \pm g$. The dipole matrix element between the $1s$ and $2p_x$ orbitals is $\langle 2p|x|1s\rangle = (\frac{2}{3})^5 4\sqrt{2}$, given the analytical functions of the two orbitals, leading to $g = (\frac{2}{3})^5 4\sqrt{2}\lambda\sqrt{\omega_0}$ in the resonance condition. For $\lambda = 0.05$, $g = 0.01613$ $(= 0.4389\,\text{eV})$. The polaritonic energies obtained from the JC model for this scenario are also shown in Fig. 3(b). Our QEDFT results at a coupling parameter of 0.05 align with those derived from the JC model. However, discrepancies emerge in the strong-coupling regime $(\lambda = 0.1)$, where our QEDFT results show an asymmetric Rabi splitting, a feature absent in the JC model. Asymmetric Rabi splitting in the strong-coupling regime naturally arises also in other *ab initio* spectra [44,45], and can also be observed and studied experimentally [46].

IV. CONCLUSION AND OUTLOOK

In summary, we have explored the reliability of px and pxLDA approximations, which are based on expressing the quantum fluctuations of the photons by the quantum-matter fluctuations, across various dimensional systems, coupling parameters, and frequency regimes. While designed for ultrastrong coupling, these nonperturbative approximations can achieve accuracy in weak-coupling situations by incorporating renormalization factors that take electron-photon correlation contributions into account. We demonstrated the efficiency of these methods in recovering both qualitative and quantitative exact results. Moreover, we established connections between changes in optical spectra and modifications in the ground state of strongly coupled light-matter systems. Accessing both static and time-dependent observables, such as changes in ground-state densities and optical spectra, within a unified theoretical framework opens up a lot of intriguing possibilities to explore in more detail the modifications of chemical and material equilibrium properties as uncovered by seminal experimental investigations in polaritonic chemistry and materials science [5,6,10,14,47,48]. This

[4]In SI units, $g = \mathbf{d}\cdot\boldsymbol{\varepsilon}\sqrt{\omega/2\hbar\varepsilon_0 V} = \mathbf{d}\cdot\boldsymbol{\varepsilon}(\lambda/\hbar)\sqrt{\omega/2}$, where $\lambda = \sqrt{\hbar/\epsilon_0 V}$ and V the mode volume.

underscores the potential of *ab initio* QED methods, particularly QEDFT, for future applications to the control of chemical and materials processes in cavities of tailored quantum environments. Our study demonstrates that even simple approximate functionals yield qualitatively correct results and can be systematically improved, not only qualitatively but also quantitatively, through comparative analysis.

Here we concentrated on simple finite systems to thoroughly examine the reliability of various approximate functionals. Unlike the often-employed unitarily equivalent length form of the PF Hamiltonian [17,49–51], the presented approximations, grounded in the velocity gauge, offer direct applicability to extended systems, setting the stage for their application to solids. The velocity gauge provides a direct connection to full minimal-coupling considerations, with a complete minimal-coupling form of the px potential already established in the literature [25]. Exploring this approach for the full minimal-coupling PF Hamiltonian within the Maxwell-Pauli-Kohn-Sham framework [31] and considering functionals for chiral cavities [3,16] represent promising future directions.

Beyond ground-state scenarios, the development of nonadiabatic (current-)density functionals is crucial. Leveraging the local-force equation, similar to (electron-only) time-dependent DFT, offers a viable strategy [32,33]. Future research will also involve extensive benchmarking of existing approximate QEDFT functionals. While benchmarks for standard electronic-structure methods are well established, reliable reference results for polaritonic systems, especially in realistic contexts, are still in progress. This challenge extends beyond single molecules and atoms to collectively coupled systems [17,51–55], where the nonperturbative interplay between electronic and rovibrational degrees of freedom in large ensembles presents intriguing possibilities [10,56,57]. Exploring these interactions could unveil novel avenues for electronic-structure methods by bridging disparate energy and length scales.

ACKNOWLEDGMENTS

This work was supported by the Cluster of Excellence "CUI:Advanced Imaging of Matter" of the Deutsche Forschungsgemeinschaft (DFG), EXC 2056, Grupos Consolidados (IT1453-22) and SFB925. I.-T. Lu thanks the Alexander von Humboldt-Stiftung for the financial support from Humboldt Research Fellowship. The authors thank Dr. C. Schäfer, Dr. J. Flick, Dr. D. M. Welakuh, Dr. H. Appel, Dr. L. Weber, and I. Ahmadabadi for the fruitful discussions. I.-T. Lu thanks Dr. D. M. Welakuh for providing an in-house (private) python version of LibQED, which has been developed by previous and current members in Prof. A. Rubio's research group, to solve the nonrelativistic PF Hamiltonian via the exact diagonalization. The Flatiron Institute is a division of the Simons Foundation.

APPENDIX A: DERIVATION FOR THE PAULI-FIERZ HAMILTONIAN WITH THE DRESSED PHOTON MODES

After the expansion of the kinetic energy term in Eq. (1), the PF Hamiltonian can be written as the sum of (1) the Hamiltonian for the matter $\hat{H}_{\mathrm{M}}$, (2) the Hamiltonian for the photon system $\hat{H}_\gamma$, and (3) the interaction between the two systems $\frac{1}{c}\hat{\mathbf{A}}\cdot\hat{\mathbf{J}}_{\mathrm{p}}$ with the paramagnetic current operator $\hat{\mathbf{J}}_{\mathrm{p}}=\sum_{l=1}^{N_e}(-i\boldsymbol{\nabla}_l)$:

$$\hat{H}_{\mathrm{PF}}=\hat{H}_{\mathrm{M}}+\frac{1}{c}\hat{\mathbf{A}}\cdot\hat{\mathbf{J}}_{\mathrm{p}}+\hat{H}_\gamma,$$

where the Hamiltonian for the matter system is defined as

$$\hat{H}_{\mathrm{M}}=-\frac{1}{2}\sum_{l=1}^{N_e}\nabla_l^2+\sum_{l=1}^{N_e}v_{\mathrm{ext}}(\mathbf{r}_l)+\frac{1}{2}\sum_{l\neq k}^{N_e}w(\mathbf{r}_l,\mathbf{r}_k),$$

while that for the photon system is

$$\hat{H}_\gamma=\sum_{\alpha=1}^{M_p}\omega_\alpha\left(\hat{a}_\alpha^\dagger\hat{a}_\alpha+\frac{1}{2}\right)+\frac{N_e}{2c^2}\hat{\mathbf{A}}^2,$$

where only in this Appendix we overload the notation $\hat{H}_\gamma$ for many modes, compared to the one in the main text. Here we introduce a pair of harmonic coordinates for the bare photons:

$$\hat{q}_\alpha=\frac{1}{\sqrt{2\omega_\alpha}}(\hat{a}_\alpha^\dagger+\hat{a}_\alpha),$$
$$\hat{p}_\alpha=i\sqrt{\frac{\omega_\alpha}{2}}(\hat{a}_\alpha^\dagger-\hat{a}_\alpha),$$

and rewrite $\hat{H}_\gamma$ in terms of the harmonic coordinates as

$$\begin{aligned}\hat{H}_\gamma&=\frac{1}{2}\sum_{\alpha=1}^{M_p}\left(\hat{p}_\alpha^2+\hat{q}_\alpha\sum_{\alpha'=1}^{M_p}W_{\alpha\alpha'}\hat{q}_{\alpha'}\right)\\&=\frac{1}{2}(\hat{\mathbf{P}}^{\intercal}\hat{\mathbf{P}}+\hat{\mathbf{Q}}^{\intercal}\mathbf{W}\hat{\mathbf{Q}}),\end{aligned}\tag{A1}$$

where we introduce a few notations to simplify the Hamiltonian: $\hat{\mathbf{P}}=(\hat{p}_1,\ldots,\hat{p}_{M_p})^{\intercal}$ ($\intercal$ means transpose), $\hat{\mathbf{Q}}=(\hat{q}_1,\ldots,\hat{q}_{M_p})^{\intercal}$, and $W_{\alpha\alpha'}=\omega_\alpha^2\delta_{\alpha\alpha'}+N_e\lambda_\alpha\lambda_{\alpha'}\boldsymbol{\varepsilon}_\alpha\cdot\boldsymbol{\varepsilon}_{\alpha'}$. The matrix $\mathbf{W}$ is real and symmetric, and can be diagonalized using an orthonormal matrix $\mathbf{U}$, such that $\tilde{\boldsymbol{\Omega}}=\mathbf{U}\mathbf{W}\mathbf{U}^{\mathbf{T}}$ with eigenvalues $\tilde{\omega}_\alpha^2$, where $\tilde{\omega}_\alpha$ is the dressed frequency for the αth photon mode. Next, we use a pair of transformed harmonic coordinates $\hat{\tilde{\mathbf{P}}}=\mathbf{U}\hat{\mathbf{P}}$ and $\hat{\tilde{\mathbf{Q}}}=\mathbf{U}\hat{\mathbf{Q}}$, that is, $\hat{\tilde{p}}_\alpha=\sum_{\beta=1}^{M_p}U_{\alpha\beta}\hat{p}_\beta$ and $\hat{\tilde{q}}_\alpha=\sum_{\beta=1}^{M_p}U_{\alpha\beta}\hat{q}_\beta$, respectively. The Hamiltonian for the photon system $\hat{H}_\gamma$ [Eq. (A1)] becomes, with the help of the identity $\mathbf{I}=\mathbf{U}^{\intercal}\mathbf{U}$,

$$\hat{H}_\gamma=\frac{1}{2}\sum_{\alpha=1}^{M_p}(\hat{\tilde{p}}_\alpha^2+\tilde{\omega}_\alpha^2\hat{\tilde{q}}_\alpha^2)=\sum_{\alpha=1}^{M_p}\tilde{\omega}_\alpha\left(\hat{\tilde{a}}_\alpha^\dagger\hat{\tilde{a}}_\alpha+\frac{1}{2}\right),$$

where in the second equality we define the annihilation $\hat{\tilde{a}}_\alpha$ and creation operator $\hat{\tilde{a}}_\alpha^\dagger$ for the dressed photons as

$$\hat{\tilde{a}}_\alpha=\frac{1}{\sqrt{2\tilde{\omega}_\alpha}}(\tilde{\omega}_\alpha\hat{\tilde{q}}_\alpha+i\hat{\tilde{p}}_\alpha),$$
$$\hat{\tilde{a}}_\alpha^\dagger=\frac{1}{\sqrt{2\tilde{\omega}_\alpha}}(\tilde{\omega}_\alpha\hat{\tilde{q}}_\alpha-i\hat{\tilde{p}}_\alpha).$$

Since we now use the dressed photons instead of the bare photons, the vector potential operator $\hat{\mathbf{A}}$ needs to be rewritten

in terms of the dressed photons as well:

$$\hat{\mathbf{A}} = c\sum_{\alpha=1}^{M_p}\lambda_\alpha \boldsymbol{\varepsilon}_\alpha \hat{q}_\alpha = c\sum_{\alpha=1}^{M_p}\lambda_\alpha \boldsymbol{\varepsilon}_\alpha \sum_{\beta=1}^{M_p} U_{\beta\alpha}\hat{\tilde{q}}_\beta$$
$$= c\sum_{\alpha=1}^{M_p}\left[\sum_{\beta=1}^{M_p} U_{\alpha\beta}\lambda_\beta \boldsymbol{\varepsilon}_\beta\right]\hat{\tilde{q}}_\alpha = c\sum_{\alpha=1}^{M_p}\tilde{\lambda}_\alpha \tilde{\boldsymbol{\varepsilon}}_\alpha \hat{\tilde{q}}_\alpha = \hat{\tilde{\mathbf{A}}},$$

where we define the coupling $\tilde{\lambda}_\alpha$ and polarization $\tilde{\boldsymbol{\varepsilon}}_\alpha$ for each dressed photon mode using the relation

$$\tilde{\lambda}_\alpha \tilde{\boldsymbol{\varepsilon}}_\alpha = \sum_{\beta=1}^{M_p} U_{\alpha\beta}\lambda_\beta \boldsymbol{\varepsilon}_\beta. \tag{A2}$$

The polarizations for each bare and each dressed photon mode, $\boldsymbol{\varepsilon}_\alpha$ and $\tilde{\boldsymbol{\varepsilon}}_\alpha$, are normalized, i.e., $|\boldsymbol{\varepsilon}_\alpha| = |\tilde{\boldsymbol{\varepsilon}}_\alpha| = 1$. Using this property, one can obtain the coupling $\tilde{\lambda}_\alpha$ for the αth dressed photon mode. If we assume that all the photon modes have the same coupling parameter, then the polarization for each dressed photon mode becomes $\tilde{\boldsymbol{\varepsilon}}_\alpha = \sum_{\beta=1}^{M_p} U_{\alpha\beta}\boldsymbol{\varepsilon}_\beta$, which reproduces the results in Ref. [58]. However, if the coupling parameters are different, then one should use Eq. (A2) to get the correct polarization instead. Note that the vector potential operator does not transform via the unitary matrix but expresses itself in terms of the dressed photon modes. Therefore, the PF Hamiltonian [Eq. (1)] in terms of the dressed photon modes becomes Eq. (2).

APPENDIX B: ELECTRON-PHOTON EXCHANGE POTENTIAL FOR ONE ELECTRON COUPLED TO ONE PHOTON MODE

Here we focus on the px potential for one effective photon mode. For many cavity-modes cases, we can add similar px potentials together with the corresponding light-matter coupling $\tilde{\lambda}_\alpha$ and dressed photon frequency $\tilde{\omega}_\alpha$, i.e., $v_{\mathrm{px}}(\mathbf{r}) = \sum_{\alpha=1}^{M_p} v_{\mathrm{px},\alpha}(\mathbf{r})$, where $v_{\mathrm{px},\alpha}(\mathbf{r})$ is the px potential for the αth photon mode.

Assume that the wave function of the ground state $\psi_0(\mathbf{r}) = \rho^{1/2}(\mathbf{r})$ is real, the px potential for one-electron cases can be obtained analytically from the Poisson equation (10), together with the definition of the paramagnetic current operator $\hat{\mathbf{J}}_{\mathrm{p}}$, the paramagnetic current density $\hat{\mathbf{j}}_{\mathrm{p}}(\mathbf{r})$, and $N_e = 1$:

$$\nabla^2 v_{\mathrm{px}}(\mathbf{r}) = -\frac{\tilde{\lambda}^2}{\tilde{\omega}^2}\nabla\cdot\left[\frac{(\tilde{\boldsymbol{\varepsilon}}\cdot\nabla)\langle(\tilde{\boldsymbol{\varepsilon}}\cdot\hat{\mathbf{J}}_{\mathrm{p}})\hat{\mathbf{j}}_{\mathrm{p}}(\mathbf{r})\rangle_{\psi_0}}{\rho(\mathbf{r})}\right]$$
$$= \frac{\tilde{\lambda}^2}{2\tilde{\omega}^2}\nabla^2\left[\frac{(\tilde{\boldsymbol{\varepsilon}}\cdot\nabla)^2\psi_0(\mathbf{r})}{\psi_0(\mathbf{r})}\right].$$

Thus, the px potential is

$$v_{\mathrm{px}}(\mathbf{r}) = \frac{\tilde{\lambda}^2}{2\tilde{\omega}^2}\frac{(\tilde{\boldsymbol{\varepsilon}}\cdot\nabla)^2\rho^{\frac{1}{2}}(\mathbf{r})}{\rho^{\frac{1}{2}}(\mathbf{r})}.$$

APPENDIX C: ELECTRON-PHOTON EXCHANGE ENERGY WITHIN THE LOCAL-DENSITY APPROXIMATION

Here we derive the px energy within the local-density approximation [Eq. (17)] from two approaches, the reduced density matrix (RDM) and the virial relation.

1. Derivation from the reduced density matrix

We follow a similar strategy to derive the px energy within the local-density approximation as the pxLDA force derived in Ref. [25]. First, we define the one-particle and two-particle RDM for the Slater determinant $\Phi(\mathbf{r}_1,\mathbf{r}_2,\mathbf{r}_3,\ldots,\mathbf{r}_{N_e}) = \Phi(\mathbf{r}_1,\underline{\mathbf{r}}) = \Phi(\mathbf{r}_1,\mathbf{r}_2,\underline{\underline{\mathbf{r}}})$, where we use $\underline{\mathbf{r}} = (\mathbf{r}_2,\mathbf{r}_3,\ldots,\mathbf{r}_{N_e})$ and $\underline{\underline{\mathbf{r}}} = (\mathbf{r}_3,\mathbf{r}_4,\ldots,\mathbf{r}_{N_e})$. The one-particle RDM (1RDM) is defined as

$$\rho_{(1)}(\mathbf{r}_1,\mathbf{r}_1') = N_e\int d\underline{\mathbf{r}}\,\Phi(\mathbf{r}_1,\underline{\mathbf{r}})\Phi^*(\mathbf{r}_1',\underline{\mathbf{r}}),$$

while the two-particle RDM (2RDM) is defined as

$$\rho_{(2)}(\mathbf{r}_1,\mathbf{r}_2;\mathbf{r}_1',\mathbf{r}_2') = \frac{N_e(N_e-1)}{2}\int d\underline{\underline{\mathbf{r}}}\,\Phi(\mathbf{r}_1,\mathbf{r}_2,\underline{\underline{\mathbf{r}}})\Phi^*(\mathbf{r}_1',\mathbf{r}_2',\underline{\underline{\mathbf{r}}}).$$

Using the above formula for the 1RDM and 2RDM (with the closed-shell assumption), we can write the expectation value of the current-current correlation in Eq. (16) as

$$\langle(\tilde{\boldsymbol{\varepsilon}}_\alpha\cdot\hat{\mathbf{J}}_{\mathrm{p}})\Phi|(\tilde{\boldsymbol{\varepsilon}}_\alpha\cdot\hat{\mathbf{J}}_{\mathrm{p}})\Phi\rangle = N_e\int d\mathbf{r}_1\int d\underline{\mathbf{r}}[(\tilde{\boldsymbol{\varepsilon}}_\alpha\cdot\nabla_1)\Phi(\mathbf{r}_1,\underline{\mathbf{r}})]^*[(\tilde{\boldsymbol{\varepsilon}}_\alpha\cdot\nabla_1)\Phi(\mathbf{r}_1,\underline{\mathbf{r}})]$$
$$+ N_e(N_e-1)\int d\mathbf{r}_1\int d\mathbf{r}_2\int d\underline{\underline{\mathbf{r}}}[(\tilde{\boldsymbol{\varepsilon}}_\alpha\cdot\nabla_2)\Phi(\mathbf{r}_1,\mathbf{r}_2,\underline{\underline{\mathbf{r}}})]^*[(\tilde{\boldsymbol{\varepsilon}}_\alpha\cdot\nabla_1)\Phi(\mathbf{r}_1,\mathbf{r}_2,\underline{\underline{\mathbf{r}}})]$$
$$= \int d\mathbf{r}_1(\tilde{\boldsymbol{\varepsilon}}_\alpha\cdot\nabla_{1'})(\tilde{\boldsymbol{\varepsilon}}_\alpha\cdot\nabla_1)\rho_{(1)}(\mathbf{r}_1,\mathbf{r}_1')|_{\mathbf{r}_1'=\mathbf{r}_1}$$
$$+ 2\int d\mathbf{r}_1\int d\mathbf{r}_2(\tilde{\boldsymbol{\varepsilon}}_\alpha\cdot\nabla_{2'})(\tilde{\boldsymbol{\varepsilon}}_\alpha\cdot\nabla_1)\rho_{(2)}(\mathbf{r}_1,\mathbf{r}_2;\mathbf{r}_1',\mathbf{r}_2')|_{\mathbf{r}_1'=\mathbf{r}_1,\mathbf{r}_2'=\mathbf{r}_2}.$$

For closed-shell Slater-determinant states, which we assume here and below, the 2RDM can be written in terms of the 1RDM as

$$\rho_{(2)}(\mathbf{r}_1,\mathbf{r}_2;\mathbf{r}_1',\mathbf{r}_2') = \tfrac{1}{2}\big[\rho_{(1)}(\mathbf{r}_1,\mathbf{r}_1')\rho_{(1)}(\mathbf{r}_2,\mathbf{r}_2') - \tfrac{1}{2}\rho_{(1)}(\mathbf{r}_1,\mathbf{r}_2')\rho_{(1)}(\mathbf{r}_2,\mathbf{r}_1')\big].$$

The 1RDM for the HEG, which we assume here, is given as

$$\rho_{(1)}(\mathbf{r}_1,\mathbf{r}_1') = \frac{2}{(2\pi)^d}\int_{|\mathbf{k}|<k_\mathrm{F}} d\mathbf{k}\, e^{i\mathbf{k}\cdot(\mathbf{r}_1-\mathbf{r}_1')},$$

where $k_\mathrm{F}(\mathbf{r}) = 2\pi[\rho(\mathbf{r})/2V_d]^{1/d}$. Within the HEG approximation, we have

$$\nabla_1\rho_{(1)}(\mathbf{r}_1,\mathbf{r}_1')|_{\mathbf{r}_1,\mathbf{r}_1'} = \frac{2i}{(2\pi)^d}\int_{|\mathbf{k}|<k_\mathrm{F}} d\mathbf{k}\,\mathbf{k} = 0.$$

Therefore, the expectation value within LDA becomes

$$\langle(\tilde{\boldsymbol{\varepsilon}}_\alpha\cdot\hat{\mathbf{J}}_\mathrm{p})^2\rangle = \int d\mathbf{r}_1\frac{2}{(2\pi)^d}\int_{|\mathbf{k}|<k_\mathrm{F}} d\mathbf{k}(\tilde{\boldsymbol{\varepsilon}}_\alpha\cdot\mathbf{k})^2 - \int d\mathbf{r}_1\frac{2}{(2\pi)^d}\int_{|\mathbf{k}|<\min(k_\mathrm{F},k_\mathrm{F}')} d\mathbf{k}(\tilde{\boldsymbol{\varepsilon}}_\alpha\cdot\mathbf{k})^2.$$

For the HEG, $k_\mathrm{F}' = k_\mathrm{F}$, the expectation value vanishes as expected. For an inhomogeneous medium, $\min(k_\mathrm{F},k_\mathrm{F}')$ approaches zero because k_F' can possibly get small. Therefore, we propose the following formula for the px energy within the LDA approximation:

$$E_\mathrm{pxLDA} = \int d\mathbf{r}\left(\sum_{\alpha=1}^{M_p}\frac{-\tilde{\lambda}_\alpha^2}{2\tilde{\omega}_\alpha^2}\right)\left[\frac{2\kappa}{(2\pi)^d}\int_{|\mathbf{k}|<k_\mathrm{F}} d\mathbf{k}(\tilde{\boldsymbol{\varepsilon}}_\alpha\cdot\mathbf{k})^2\right],$$

where we introduce a factor $\kappa\in[0,1]$ where $\kappa=0$ for the HEG and $\kappa=1$ for the maximally inhomogeneous limit to take all situations into account. We use the maximally inhomogeneous limit ($\kappa=1$) in this work. One can recover other scenarios by including the factor κ. The square brackets in the formula for the pxLDA energy can be evaluated in the polar coordinates in d dimension:

$$\frac{2}{(2\pi)^d}\int_{|\mathbf{k}|<k_\mathrm{F}} d\mathbf{k}(\tilde{\boldsymbol{\varepsilon}}_\alpha\cdot\mathbf{k})^2 = \frac{2V_d}{(2\pi)^d}\frac{k_\mathrm{F}^{d+2}(\mathbf{r})}{d+2}.$$

The px energy within the LDA becomes

$$E_\mathrm{pxLDA} = \left(\sum_{\alpha=1}^{M_p}\frac{-\tilde{\lambda}_\alpha^2}{\tilde{\omega}_\alpha^2}\right)\frac{2\pi^2}{d+2}\left(\frac{1}{2V_d}\right)^{\frac{2}{d}}\int d\mathbf{r}\,\rho^{\frac{2+d}{d}}(\mathbf{r}). \quad \text{(C1)}$$

Using the above pxLDA energy, we can obtain the *isotropic* pxLDA potential via the functional derivative with respect to the density as

$$v_\mathrm{pxLDA}^\mathrm{iso}(\mathbf{r}) = \left(\sum_{\alpha=1}^{M_p}\frac{-2\pi^2\tilde{\lambda}_\alpha^2}{d\tilde{\omega}_\alpha^2}\right)\left[\frac{\rho(\mathbf{r})}{2V_d}\right]^{\frac{2}{d}}.$$

Note that if we take the above isotropic pxLDA potential into the KS equations, we would lose the information of the polarization direction of those photon modes when solving the KS equations. However, if we take the pxLDA potential obtained from the force balance equation to compute the density, then we compute the pxLDA energy using Eq. (C1), which implicitly contains the information of the polarizations of those photon modes.

2. Derivation from the virial relation

The electron-photon exchange force (and its LDA version) is

$$\mathbf{F}_\mathrm{px(LDA)}(\mathbf{r}) = \sum_{\alpha=1}^{M_p}\frac{\tilde{\lambda}_\alpha^2}{\tilde{\omega}_\alpha^2}(\tilde{\boldsymbol{\varepsilon}}_\alpha\cdot\nabla)\mathbf{f}_{\alpha,\mathrm{px(LDA)}}(\mathbf{r}),$$

where $\mathbf{f}_{\alpha,\mathrm{pxLDA}}(\mathbf{r})$ [Eq. (14)] is rewritten in terms of electron density:

$$\mathbf{f}_{\alpha,\mathrm{pxLDA}}(\mathbf{r}) = \frac{(2\pi)^2}{d+2}\rho(\mathbf{r})\left[\frac{\rho(\mathbf{r})}{2V_d}\right]^{\frac{2}{d}}\tilde{\boldsymbol{\varepsilon}}_\alpha.$$

The pxLDA energy can be obtained using the virial relation (with a factor of $\frac{1}{2}$ due to the photon-energy counterterm) as

$$\begin{aligned}E_\mathrm{pxLDA} &= \frac{1}{2}\int d\mathbf{r}\,\mathbf{r}\cdot\mathbf{F}_\mathrm{pxLDA}(\mathbf{r})\\ &= \frac{1}{2}\frac{(2\pi)^2}{d+2}\sum_{\alpha=1}^{M_p}\frac{\tilde{\lambda}_\alpha^2}{\tilde{\omega}_\alpha^2}\int d\mathbf{r}(\tilde{\boldsymbol{\varepsilon}}_\alpha\cdot\mathbf{r})(\tilde{\boldsymbol{\varepsilon}}_\alpha\cdot\nabla)\\ &\quad\times\left[\rho(\mathbf{r})\left(\frac{\rho(\mathbf{r})}{2V_d}\right)^{\frac{2}{d}}\right]\\ &= \left(\sum_{\alpha=1}^{M_p}\frac{-\tilde{\lambda}_\alpha^2}{\tilde{\omega}_\alpha^2}\right)\frac{2\pi^2}{d+2}\left(\frac{1}{2V_d}\right)^{\frac{2}{d}}\int d\mathbf{r}\,\rho^{\frac{2+d}{d}}(\mathbf{r}),\end{aligned}$$

where we use integration by parts in the last line. The px energy obtained from the virial relation is the same as the one obtained from the RDM approach.

Here is a side note regarding the total px force (and its LDA version): it satisfies the zero-force condition, i.e.,

$$\begin{aligned}&\int_\Omega d\mathbf{r}\,\mathbf{F}_\mathrm{px}(\mathbf{r})\\ &= \sum_{\alpha=1}^{M_p}\frac{\tilde{\lambda}_\alpha^2}{\tilde{\omega}_\alpha^2}\int_\Omega d\mathbf{r}(\tilde{\boldsymbol{\varepsilon}}_\alpha\cdot\nabla)\mathbf{f}_{\alpha,\mathrm{px}}(\mathbf{r})\\ &= \sum_{\alpha=1}^{M_p}\frac{\tilde{\lambda}_\alpha^2}{\tilde{\omega}_\alpha^2}\int_\Omega d\mathbf{r}\{\nabla[\tilde{\boldsymbol{\varepsilon}}_\alpha\cdot\mathbf{f}_{\alpha,\mathrm{px}}(\mathbf{r})] - \tilde{\boldsymbol{\varepsilon}}_\alpha[\nabla\times\mathbf{f}_{\alpha,\mathrm{px}}(\mathbf{r})]\}\\ &= \sum_{\alpha=1}^{M_p}\frac{\tilde{\lambda}_\alpha^2}{\tilde{\omega}_\alpha^2}\left[\int_{\partial\Omega} d\mathbf{S}\,\tilde{\boldsymbol{\varepsilon}}_\alpha\cdot\mathbf{f}_{\alpha,\mathrm{px}}(\mathbf{r}) - \tilde{\boldsymbol{\varepsilon}}_\alpha\int_{\partial\Omega} d\mathbf{S}\times\mathbf{f}_{\alpha,\mathrm{px}}(\mathbf{r})\right]\\ &= 0, \qquad \text{(C2)}\end{aligned}$$

where Ω is the volume of interest and its surface $\partial\Omega$. In the second line of Eq. (C2), we use the vector calculus identity $\nabla(\mathbf{A}\cdot\mathbf{B}) = (\mathbf{A}\cdot\nabla)\mathbf{B} + (\mathbf{B}\cdot\nabla)\mathbf{A} + \mathbf{A}\times(\nabla\times\mathbf{B}) + \mathbf{B}\times(\nabla\times\mathbf{A})$ where $\mathbf{A} = \tilde{\boldsymbol{\varepsilon}}_\alpha$ and $\mathbf{B} = \mathbf{f}_{\alpha,\mathrm{px}}(\mathbf{r})$. In the third line of Eq. (C2), we use the following two identities: (1) $\int_\Omega d\mathbf{r}\,\nabla\phi(\mathbf{r}) = \int_{\partial\Omega} d\mathbf{S}\,\phi(\mathbf{r})$, where $\phi(\mathbf{r})$ is a scalar function, and (2) $\int_\Omega d\mathbf{r}\,\nabla\times\mathbf{A}(\mathbf{r}) = \int_{\partial\Omega} d\mathbf{S}\times\mathbf{A}(\mathbf{r})$, where $\mathbf{A}$ is a vector-valued function. In the last line of Eq. (C2), the surface integrals vanish in both finite and periodic systems. More detailed discussions on subtle virial-relation issues can be found in works addressing force-based functionals in standard electron-only density-functional theory, such as Ref. [33].

APPENDIX D: COMPUTATIONAL DETAILS

For the exact diagonalization method, the ground-state electron density $\rho^{\text{exact}}(\mathbf{r})$ is obtained by tracing out the photon-Fock space $\rho^{\text{exact}}(\mathbf{r}) = \sum_{n=1}^{n_{\max}} \Psi_0^*(\mathbf{r}, n)\Psi_0(\mathbf{r}, n)$, where $\Psi_0(\mathbf{r}, n)$ is the ground-state wave function of the PF Hamiltonian with one-photon mode [Eq. (18)], n the number of photon-Fock states, and $n_{\max}$ the maximum number of Fock states we choose to converge the energies of the ground state and a few excited states for tunable light-matter couplings λ. For the HO, we use a 301-point grid centered at the origin with a grid spacing of $\Delta x = 0.07$ bohrs. In the case of the quantum ring, we use a 61×61 grid centered at the origin with a step size of $\Delta x = 0.2$ bohrs. To achieve convergence, we use $n_{\max} = 20$ and apply a fourth-order finite-difference scheme for the real-space derivatives on the grid, including the Laplacian operator for kinetic energy.

The pxLDA functional [Eq. (15)], together with the one-electron px [Eq. (13)] and the renormalization factors η_c, are implemented in the open-source code OCTOPUS [34]. In QEDFT approaches, we use specific real-space grid sizes and box dimensions for different systems: HO (grid size $\Delta x = 0.07$ bohrs, length 21 bohrs), quantum ring (grid size $\Delta x = 0.2$ bohrs, length 20 bohrs), and the hydrogen atom (grid size $\Delta x = 0.24$ bohrs, radius 20 bohrs). For the OEP functional in exchange approximation, we solve the KS equation with the potential obtained from solving the full OEP equation [22].

In QEDFT, we self-consistently solve the KS equation for the ground state. To calculate the optical spectrum for the hydrogen case using OCTOPUS, we employ time-dependent techniques, propagating the ground-state wave function with the KS Hamiltonian, i.e., Eq. (3) with the adiabatic KS potential approximations. The optical spectrum is obtained by Fourier transforming the time-dependent dipole moment, which is computed using the delta-kick method with a kick strength of 0.01 Å. The time propagation extends for 50 fs (2067 atomic units) with a time step of approximately 0.0019 fs (0.08 atomic unit).

APPENDIX E: A MANY-ELECTRON CASE: THE ATOM INSIDE A CAVITY

To simulate a system with many electrons inside a cavity using the QEDFT approach, we require an approximate mean-field exchange-correlation potential for the KS potential, given by $v_{\text{KS}}(\mathbf{r}) = v_{\text{ext}}(\mathbf{r}) + v_{\text{Mxc}}(\mathbf{r})$. The approximated mean-field exchange-correlation potential $v_{\text{Mxc}}(\mathbf{r})$ consists of the Hartree potential $v_{\text{H}}(\mathbf{r})$, the electron-electron exchange-correlation potential $v_{\text{xc}}(\mathbf{r})$, and the electron-photon exchange potential $v_{\text{px}}(\mathbf{r})$, that is, $v_{\text{Mxc}}(\mathbf{r}) \approx v_{\text{H}}(\mathbf{r}) + v_{\text{xc}}(\mathbf{r}) + v_{\text{px}}(\mathbf{r})$. Various methods [37,38], such as LDA, generalized gradient approximation, and OEP, can be used to approximate and compute $v_{\text{xc}}(\mathbf{r})$, while $v_{\text{px}}(\mathbf{r})$ can be approximated using OEP [22] or the method developed in this work. The external potential $v_{\text{ext}}(\mathbf{r})$, representing the interaction between nuclei and electrons, is typically modeled using pseudopotentials [38].

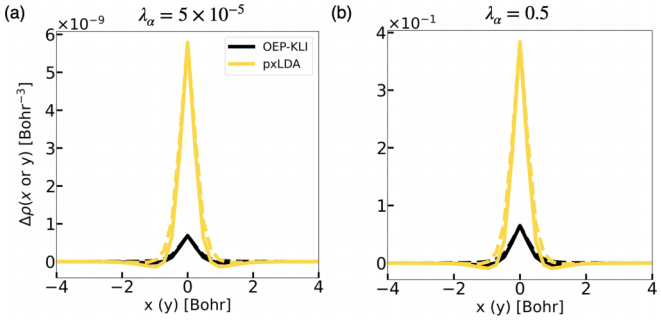

FIG. 4. The photon mode is polarized along the x direction and a photon frequency of 0.839 27 hartree, in resonance with the transition between the $1s$ and $2p$ orbitals of the He atom outside the cavity. (a), (b) The electron-density differences $\Delta\rho$ along the x (solid lines) and y (dashed lines) directions in the weak- and strong-coupling regimes, computed using the OEP-KLI and pxLDA approximations for the electron-photon interaction. The electron-electron exchange potential is approximated and solved using the OEP-KLI approach, while the electron-electron correlation potential is approximated and obtained using the LDA approach.

We illustrate our approach using a helium (He) atom as a representative example of many-electron systems within an optical cavity. The He atom is treated with the OCTOPUS open-source code [34], using a radius of 30 bohrs and a real-space grid size of 0.24 bohrs. The Hartwigsen-Goedecker-Hutter LDA pseudopotential [59] models the interaction of the valence electrons with the nuclei, while the electron-electron interaction among the valence electrons is handled using the OEP method with the Krieger-Li-Iafrate (KLI) approximation for the exchange potential [60] and LDA for the correlation potential [61]. Our primary focus is on the electron-photon interaction, specifically the electron-photon exchange potential. We use the OEP within the KLI approximation as a reference[5] for realistic systems in the weak-coupling regime [22], comparing it with our pxLDA potential. Figure 4 shows the electron-density difference of the He atom inside and outside the cavity for both small and large light-matter couplings. In the weak-coupling regime, our pxLDA results show an overestimation of electron density compared to the OEP method, akin to the hydrogen case. This example underscores the versatility of our pxLDA approach in extending to many-electron systems, incorporating the electron-electron exchange-correlation potential in the KS potential.

[5]The OEP-KLI results are close to the OEP results.

[1] M. Ruggenthaler, J. Flick, C. Pellegrini, H. Appel, I. V. Tokatly, and A. Rubio, Phys. Rev. A **90**, 012508 (2014).

[2] M. Ruggenthaler, N. Tancogne-Dejean, J. Flick, H. Appel, and A. Rubio, Nat. Rev. Chem. **2**, 0118 (2018).

[3] H. Hübener, U. De Giovannini, C. Schäfer, J. Andberger, M. Ruggenthaler, J. Faist, and A. Rubio, Nat. Mater. **20**, 438 (2021).

[4] J. Flick, M. Ruggenthaler, H. Appel, and A. Rubio, Proc. Natl. Acad. Sci. USA **114**, 3026 (2017).

[5] F. J. Garcia-Vidal, C. Ciuti, and T. W. Ebbesen, Science **373**, eabd0336 (2021).

[6] T. W. Ebbesen, Acc. Chem. Res. **49**, 2403 (2016).

[7] M. A. Sentef, M. Ruggenthaler, and A. Rubio, Sci. Adv. **4**, eaau6969 (2018).

[8] Y. Ashida, A. İmamoğlu, J. Faist, D. Jaksch, A. Cavalleri, and E. Demler, Phys. Rev. X **10**, 041027 (2020).

[9] S. Latini, D. Shin, S. A. Sato, C. Schäfer, U. De Giovannini, H. Hübener, and A. Rubio, Proc. Natl. Acad. Sci. USA **118**, e2105618118 (2021).

[10] F. Schlawin, D. M. Kennes, and M. A. Sentef, Appl. Phys. Rev. **9**, 011312 (2022).

[11] G. Jarc, S. Y. Mathengattil, A. Montanaro, F. Giusti, E. M. Rigoni, R. Sergo, F. Fassioli, S. Winnerl, S. Dal Zilio, D. Mihailovic, P. Prelovšek, M. Eckstein, and D. Fausti, Nature (London) **622**, 487 (2023).

[12] D. M. Kennes and A. Rubio, in *Sketches of Physics: The Celebration Collection*, Lecture Notes in Physics, edited by R. Citro, M. Lewenstein, A. Rubio, W. P. Schleich, J. D. Wells, and G. P. Zank (Springer, Cham, 2023), pp. 1–39.

[13] P. Forn-Díaz, L. Lamata, E. Rico, J. Kono, and E. Solano, Rev. Mod. Phys. **91**, 025005 (2019).

[14] A. Frisk Kockum, A. Miranowicz, S. De Liberato, S. Savasta, and F. Nori, Nat. Rev. Phys. **1**, 19 (2019).

[15] J. Flick, N. Rivera, and P. Narang, Nanophotonics **7**, 1479 (2018).

[16] R. R. Riso, L. Grazioli, E. Ronca, T. Giovannini, and H. Koch, Phys. Rev. X **13**, 031002 (2023).

[17] M. Ruggenthaler, D. Sidler, and A. Rubio, Chem. Rev. **123**, 11191 (2023).

[18] I. V. Tokatly, Phys. Rev. Lett. **110**, 233001 (2013).

[19] J. Flick, M. Ruggenthaler, H. Appel, and A. Rubio, Proc. Natl. Acad. Sci. USA **112**, 15285 (2015).

[20] C. Pellegrini, J. Flick, I. V. Tokatly, H. Appel, and A. Rubio, Phys. Rev. Lett. **115**, 093001 (2015).

[21] J. Flick, Phys. Rev. Lett. **129**, 143201 (2022).

[22] J. Flick, C. Schäfer, M. Ruggenthaler, H. Appel, and A. Rubio, ACS Photonics **5**, 992 (2018).

[23] J. Flick, D. M. Welakuh, M. Ruggenthaler, H. Appel, and A. Rubio, ACS Photonics **6**, 2757 (2019).

[24] D. Novokreschenov, A. Kudlis, I. Iorsh, and I. V. Tokatly, Phys. Rev. B **108**, 235424 (2023).

[25] C. Schäfer, F. Buchholz, M. Penz, M. Ruggenthaler, and A. Rubio, Proc. Natl. Acad. Sci. USA **118**, e2110464118 (2021).

[26] M. K. Svendsen, M. Ruggenthaler, H. Hübener, C. Schäfer, M. Eckstein, A. Rubio, and S. Latini, arXiv:2312.17374.

[27] M. Ruggenthaler, arXiv:1509.01417.

[28] M. Penz, E. I. Tellgren, M. A. Csirik, M. Ruggenthaler, and A. Laestadius, ACS Phys. Chem. Au **3**, 492 (2023).

[29] M. K. Svendsen, K. S. Thygesen, A. Rubio, and J. Flick, J. Chem. Theory Comput. **20**, 926 (2024).

[30] M. K. Svendsen, Y. Kurman, P. Schmidt, F. Koppens, I. Kaminer, and K. S. Thygesen, Nat. Commun. **12**, 2778 (2021).

[31] R. Jestädt, M. Ruggenthaler, M. J. T. Oliveira, A. Rubio, and H. Appel, Adv. Phys. **68**, 225 (2019).

[32] M.-L. M. Tchenkoue, M. Penz, I. Theophilou, M. Ruggenthaler, and A. Rubio, J. Chem. Phys. **151**, 154107 (2019).

[33] N. Tancogne-Dejean, M. Penz, A. Laestadius, M. A. Csirik, M. Ruggenthaler, and A. Rubio, J. Chem. Phys. **160**, 024103 (2024).

[34] N. Tancogne-Dejean, M. J. T. Oliveira, X. Andrade, H. Appel, C. H. Borca, G. Le Breton, F. Buchholz, A. Castro, S. Corni, A. A. Correa, U. De Giovannini, A. Delgado, F. G. Eich, J. Flick, G. Gil, A. Gomez, N. Helbig, H. Hübener, R. Jestädt, J. Jornet-Somoza *et al.*, J. Chem. Phys. **152**, 124119 (2020).

[35] L. Weber, E. Viñas Boström, M. Claassen, A. Rubio, and D. M. Kennes, Commun. Phys. **6**, 247 (2023).

[36] L. Weber, M. Morales, S. Zhang, and A. Rubio, *talk presented at the CMD30 FisMat2023 conference, Milano, Italy, September 4-8*, 2023 (unpublished), https://eventi.cnism.it/cmd30-fismat/submission/view/1365942206119779863.

[37] R. M. Dreizler and E. K. Gross, *Density Functional Theory* (Springer, New York, 2012).

[38] R. M. Martin, *Electronic Structure* (Cambridge University Press, Cambridge, 2020).

[39] C. A. Ullrich, *Time-Dependent Density-Functional Theory: Concepts and Applications* (Oxford University Press, Oxford, 2011).

[40] M. Ruggenthaler, M. Penz, and R. van Leeuwen, J. Phys.: Condens. Matter **27**, 203202 (2015).

[41] G. Passetti, C. J. Eckhardt, M. A. Sentef, and D. M. Kennes, Phys. Rev. Lett. **131**, 023601 (2023).

[42] V. Rokaj, M. Ruggenthaler, F. G. Eich, and A. Rubio, Phys. Rev. Res. **4**, 013012 (2022).

[43] C. Schäfer, M. Ruggenthaler, and A. Rubio, Phys. Rev. A **98**, 043801 (2018).

[44] T. Schnappinger, D. Sidler, M. Ruggenthaler, A. Rubio, and M. Kowalewski, J. Phys. Chem. Lett. **14**, 8024 (2023).

[45] T. Schnappinger and M. Kowalewski, J. Chem. Theory Comput. **19**, 9278 (2023).

[46] A. Canales, T. Karmstrand, D. G. Baranov, T. J. Antosiewicz, and T. O. Shegai, Nanophotonics **12**, 4073 (2023).

[47] D. Sanvitto and S. Kéna-Cohen, Nat. Mater. **15**, 1061 (2016).

[48] T. W. Ebbesen, A. Rubio, and G. D. Scholes, Chem. Rev. **123**, 12037 (2023).

[49] D. P. Craig and T. Thirunamachandran, *Molecular Quantum Electrodynamics: An Introduction to Radiation-Molecule Interactions* (Dover, New York, 1998).

[50] C. Schäfer, M. Ruggenthaler, V. Rokaj, and A. Rubio, ACS Photonics **7**, 975 (2020).

[51] A. Mandal, M. A. Taylor, B. M. Weight, E. R. Koessler, X. Li, and P. Huo, Chem. Rev. **123**, 9786 (2023).

[52] J. Feist, J. Galego, and F. J. Garcia-Vidal, ACS Photonics **5**, 205 (2018).

[53] T. E. Li, B. Cui, J. E. Subotnik, and A. Nitzan, Annu. Rev. Phys. Chem. **73**, 43 (2022).

[54] D. Sidler, M. Ruggenthaler, C. Schäfer, E. Ronca, and A. Rubio, J. Chem. Phys. **156**, 230901 (2022).

[55] J. A. Campos-Gonzalez-Angulo, Y. R. Poh, M. Du, and J. Yuen-Zhou, J. Chem. Phys. **158**, 230901 (2023).

[56] B. S. Simpkins, A. D. Dunkelberger, and I. Vurgaftman, Chem. Rev. **123**, 5020 (2023).

[57] K. Hirai, J. A. Hutchison, and H. Uji-i, Chem. Rev. **123**, 8099 (2023).

[58] F. H. Faisal, *Theory of Multiphoton Processes* (Springer, New York, 1987).

[59] C. Hartwigsen, S. Goedecker, and J. Hutter, Phys. Rev. B **58**, 3641 (1998).

[60] J. B. Krieger, Y. Li, and G. J. Iafrate, Phys. Lett. A **146**, 256 (1990).

[61] J. P. Perdew and A. Zunger, Phys. Rev. B **23**, 5048 (1981).